Molecular Phylogenetics and Evolution 222 (2026) 108648

Contents lists available at ScienceDirect

Molecular Phylogenetics and Evolution

journal homepage: www.elsevier.com/locate/ympev

Deciphering reticulation and reproductive trait evolution in a chasmophyte lineage: a phylogenomic approach to the evolutionary patterns within *Petrocoptis*

Jorge Calvo-Yuste [a,b,*,1], M.Montserrat Martínez-Ortega [a,b,2], Teresa Malvar Ferreras [b,3], Juan Viruel [c,d,e,4], Pablo Tejero [f,g,*,5]

[a] Área de Botánica, Universidad de Salamanca, Spain
[b] Herbario y Biobanco de ADN vegetal, Universidad de Salamanca, Spain
[c] Technological College, University of Zaragoza, Huesca, Spain
[d] Institute for Biocomputation and Physics of Complex Systems (BIFI), Zaragoza, Spain
[e] Royal Botanic Gardens, Kew, Richmond, UK
[f] Herbario JACA, Instituto Pirenaico de Ecología (IPE-CSIC), Jaca, Spain
[g] Aranzadi Society of Sciences, Donostia-San Sebastián, Spain

ARTICLE INFO

Keywords:
Caryophyllaceae
Chasmophyte
Floral trait evolution
Genomic heterozygosity
Phylogenomics
Reticulate evolution
Strophiole-mediated adaptative syndrome

ABSTRACT

The interplay between reticulate evolution and adaptive trait diversification during speciation remains a central challenge in evolutionary biology. We hypothesized that diversification in the Iberian chasmophytic genus *Petrocoptis* has been shaped by recurrent reticulation coupled with coordinated evolution of reproductive traits, including a strophiole-mediated seed adaptive syndrome linked to water uptake regulation in xeric cliff habitats.

We analysed 63 representative populations using target enrichment of 345 nuclear loci (Angiosperms353) and 192 plastid regions. Phylogenomic relationships were inferred under concatenation and multispecies coalescent frameworks, accounting for genealogical and cytonuclear discordances, ILS and reticulate evolution. Seed and floral traits were analysed within an integrative phylogenetic comparative framework that jointly assessed evolutionary patterns, genomic variation, and climatic correlates.

Cytonuclear discordance analyses and coalescent simulations rejected ILS as the unique driver of conflict. Network analyses supported at least two reticulation events, indicating ancestral hybridization. The evolution of reproductive traits displayed a framework of repeated and coordinated adaptive shifts. Floral evolution revealed multiple increases in calyx length associated with pink corollas and higher genomic heterozygosity. Seed morphology followed an ordered transition in strophiolar hair types and distinct adaptive optima: cylindrical hairs were associated with small seeds and proportionally larger strophioles, whereas claviform hairs corresponded to larger seeds with reduced relative strophioles. Strophiole traits correlated with temperature and precipitation, defining a climate-associated seed adaptive syndrome which may optimize water uptake regulation.

Together, these results highlight the joint effects of reticulate genomic evolution and adaptive restructuring of reproductive traits in *Petrocoptis* diversification. Integrating phylogenetic networks with trait evolution provides a cohesive framework for understanding how gene flow and ecological specialization jointly drive lineage diversification in fragmented cliff systems.

* Corresponding authorsat: Herbario JACA, Instituto Pirenaico de Ecología (IPE-CSIC), Jaca, Spain..
E-mail addresses: jorcaly@usal.es (J. Calvo-Yuste), mmo@usal.es (M.Montserrat Martínez-Ortega), tmalvarf@usal.es (T.M. Ferreras), viruel@unizar.es (J. Viruel), ptibarra@ipe.csic.es (P. Tejero).
[1] 0000-0002-1570-8277.
[2] 0000-0002-3887-2416.
[3] 0000-0002-2861-4595.
[4] 0000-0001-5658-8411.
[5] 0000-0001-6735-3423.

https://doi.org/10.1016/j.ympev.2026.108648
Received 2 March 2026; Received in revised form 14 May 2026; Accepted 14 May 2026
Available online 16 May 2026

1. Introduction

Understanding how biological diversity originates and is maintained requires integrating processes that operate across multiple temporal and spatial scales ranging from population divergence and local adaptation to the emergence of reproductively isolated lineages (Avise, 2000; Coyne and Orr, 2004; Schluter, 2000). In plants, diversification is often promoted by extrinsic drivers such as climatic oscillations, geological dynamics, habitat fragmentation, and biological traits that modulate dispersal, reproduction and ecological interactions (Antonelli et al., 2018; Hewitt, 2000; Hughes and Eastwood, 2006). Mountain uplift and erosion, river incision, glacial–interglacial cycles and the fragmentation of suitable habitats have repeatedly generated mosaics of isolation and secondary contact, fostering divergence from shared ancestral gene pools and, under persistent isolation or divergent selection, effective speciation (Médail and Diadema, 2009; Willis et al., 2004). These dynamics are particularly pronounced in topographically complex regions, where small, spatially restricted populations are exposed to strong ecological gradients and limited connectivity, creating conditions for rapid diversification and lineage sorting (Badgley et al., 2017; Hughes et al., 2013).

Populations originating from a common genetic background may follow independent adaptive trajectories driven by local selective pressures ultimately leading to the evolution of reproductive barriers and speciation (Coyne and Orr, 2004; Nosil, 2012; Schluter, 2000). In plants, however, speciation rarely proceeds along a simple, strictly bifurcating trajectory. Increasing evidence shows that lineage divergence frequently occurs in the presence of incomplete lineage sorting (ILS) and reticulate evolution, a broad term encompassing historical gene flow, hybridization and introgression (Degnan and Rosenberg, 2009). These processes generate complex and often conflicting genomic signatures (Maddison, 1997; Mallet et al., 2016; Pamilo and Nei, 1988; Rieseberg and Soltis, 1991). ILS arises when ancestral polymorphisms persist across successive speciation events and are randomly distributed among descendant lineages. Reticulate evolution instead reflects gene exchange among diverging or partially isolated taxa. Both processes are especially prevalent in lineages that underwent rapid radiations or experienced repeated cycles of range fragmentation and reconnection, and they pose major challenges to the reconstruction of evolutionary histories under strictly tree-like models (Cai et al., 2021; Morales-Briones et al., 2021; Seehausen, 2004; Whitfield and Lockhart, 2007).

In plants, cytonuclear discordance (i.e., conflicting phylogenetic signals between plastid and nuclear genomes) has become a hallmark of such complex evolutionary scenarios and is frequently interpreted as evidence of historical reticulation (Fehrer et al., 2007; Pirie et al., 2009; Scheunert and Heubl, 2017; Yang et al., 2023a). However, similar patterns may also result from ILS or methodological artefacts such as gene tree estimation error, making it difficult to unequivocally identify the underlying evolutionary processes (Degnan and Rosenberg, 2009; Maddison, 1997; Pamilo and Nei, 1988; Springer and Gatesy, 2016). Empirical studies increasingly report extensive conflict among independent nuclear loci, as well as between nuclear and plastid genomes, highlighting the limitations of assuming strictly bifurcating species trees in such systems (Cai et al., 2021; Morales-Briones et al., 2018; Sang et al., 1995; Soltis and Kuzoff, 1995). Disentangling the relative contributions of ILS and reticulate evolution therefore requires genome-scale datasets and analytical frameworks that explicitly model coalescent stochasticity and gene flow, including multispecies coalescent species tree methods and phylogenetic network approaches (Blair and Ané, 2020; Edwards et al., 2016; Solís-Lemus and Ané, 2016; Wen et al., 2016; Yu and Nakhleh, 2015). The application of these integrative approaches has revealed that reticulate evolution is not an exception but a recurrent feature of plant diversification, particularly in geographically structured, species-rich lineages.

Beyond genomic relationships, diversification is intimately linked to the evolution of phenotypic traits influencing the fitness (Fenster et al., 2004; Stebbins, 1970). A growing body of work shows that reproductive traits such as floral morphology, colour, and seed structures, often evolve in ways that are at least partly uncoupled from phylogenetic relationships (Smith and Kriebel, 2018; Whittall and Hodges, 2007). When trait evolution does not mirror the underlying species or population tree, closely related species or populations may exhibit strikingly divergent phenotypes (Losos, 2011). This uncoupling reflects the fact that reproductive traits are frequently subject to selective pressures (e.g., pollinator assemblages, mating systems and dispersal constraints) which may rapidly change their strength and direction (Fenster et al., 2004; Van der Niet and Johnson, 2012). In plants, floral traits can evolve quickly and independently in response to pollinator-mediated selection, generating complex evolutionary patterns that contrast with more conservative traits that track deep phylogenetic history (Armbruster, 2014). Such lability can promote reproductive isolation and contribute directly to speciation, even in the absence of long-term geographic isolation (Kay and Sargent, 2009).

Seed traits provide a complementary perspective on plant adaptive diversification. Traits related to dispersal and germination, including seed size, surface structures and appendages, are tightly linked to environmental conditions and recruitment success (Harper et al., 1970; Westoby et al., 1996). In fragmented and stressful habitats, selection on seed traits can be intense, favouring strategies that enhance establishment under limiting conditions (Moles and Westoby, 2004). Water availability is a major constraint in xeric systems and traits that modulate water uptake during germination can be critical for seedling survival (Baskin and Baskin, 2014). Water entry into seeds occurs through specific structures such as the hilum, micropyle or strophiole (Upretee et al., 2024), and is influenced by seed coat properties, seed size and the morphology of associated appendages (Baskin and Baskin, 2014). The primary pathways of water uptake and the relative permeability of these entry sites vary widely among species and depend on anatomical features of the seed coat (e.g. thickness, presence of pores or hydrophilic compounds), with seed size strongly modulating the rate and pattern of imbibition (Upretee et al., 2024). Larger seeds generally exhibit lower overall permeability due to reduced surface–to–volume ratios, whereas specialized structures such as enlarged strophioles or modified hila may facilitate localized water entry when moisture becomes available (Gutterman, 2000; Upretee et al., 2024). In some lineages, these structures are also associated with dispersal syndromes, including myrmecochory, where appendages attract ants while simultaneously influencing hydration dynamics (Lengyel et al., 2010).

Vertical cliffs impose severe constraints on pollination, dispersal and germination for strictly rupicolous plant species. These habitats are highly fragmented and function as biogeographic islands, making them ideal systems for studying plant diversification, adaptation, and speciation processes (Medail and Quezel, 1997). Pollinator interactions in cliff environments can generate complex patterns of reproductive isolation and selection on floral traits (Armbruster, 2014). Plants growing on cliffs are also exposed to intense abiotic stress, including limited soil development, discontinuous water availability and extreme microclimatic conditions, which strongly influence seed germination, seedling establishment, and survival (Larson et al., 2000). Restricted dispersal among populations reduces gene flow, but can simultaneously promote local differentiation and the evolution of adaptive traits, such as seed structures that facilitate water uptake or specialized dispersal mechanisms. Collectively, these environmental and biological constraints cause vertical cliffs to act as systems in which geographic isolation, intense selective pressures, and limited historical connectivity can drive rapid divergence and the evolution of highly specialized adaptive traits.

The Iberian endemic chasmophytic genus *Petrocoptis* A. Braun ex Endl. (Caryophyllaceae) constitutes an exceptional model to investigate how genomic complexity and reproductive trait evolution interact during plant diversification in geographically structured systems. Despite its restricted distribution, *Petrocoptis* exhibits substantial intra-

and interspecific variation in reproductive traits, including flower size, corolla colour, mating systems, seed size and strophiole morphology, all of which are of major taxonomic and ecological relevance (Merxmüller and Grau, 1968; Montserrat and Fernández-Casas, 1990; Navarro et al., 1993; Navarro and Guitián, 2002; Rothmaler, 1941; Walters, 1993). A previous study has suggested that several seed traits may represent adaptive responses to local climatic conditions (Calvo-Yuste et al., 2024). Specifically, variation in strophiole size appears to be associated with average annual rainfall and maximum temperature, supporting the hypothesis that the strophiole plays a role in seed water uptake and germination regulation (Calvo-Yuste et al., 2024), rather than serving as an attractant for ants, as proposed by other authors (Ortega-Olivencia et al., 2021). These observations point to the existence of adaptive syndromes associated with water acquisition that remain largely understudied, and are conceptually analogous to well-documented pollination or dispersal syndromes, but focused on germination ecology.

From a phylogenetic perspective, *Petrocoptis* has long proven challenging. Despite sustained interest in its systematics and ecology, evolutionary relationships among species remain poorly resolved. Earlier phylogenetic analyses based on limited number of loci revealed substantial incongruence between plastid and nuclear datasets and failed to resolve several species-level relationships (Cires and Prieto, 2015; Mayol and Rosselló, 2001). These results suggested early rapid divergence and an evolutionary history shaped by ILS and ancestral hybridization. All species of *Petrocoptis* are diploid ($2n = 24$), and there is no evidence that polyploidy contributed to diversification in the genus (Merxmüller and Grau, 1968; Montserrat and Fernández-Casas, 1990). Hybridization and ILS, rather than genome duplication, therefore represents the most plausible explanations for the observed cytonuclear discordance. However, the lack of genome-scale data has so far prevented a rigorous evaluation of these hypotheses, including formal tests of reticulate evolution and assessments of the phylogenetic structure of key reproductive traits.

The primary objective of this study is to disentangle the evolutionary history of the Iberian endemic genus *Petrocoptis*, using genome-scale nuclear and plastid data. Specifically, our first objective is to reconstruct species relationships within multispecies coalescent and network frameworks, explicitly accounting for ILS and reticulate evolution. A second objective is to reconstruct the evolutionary history of key reproductive traits, with a particular focus on floral and seed traits that are central to taxonomy, ecology, and reproductive strategies in the genus. We ask whether the variability of these traits is phylogenetically structured, whether it reflects adaptive responses to environmental and reproductive pressures, and to what extent trait evolution is associated with genomic heterogeneity and reticulation. By integrating phylogenomics, network inference, and comparative trait evolution, this study addresses how genomic complexity and reproductive trait diversification have jointly shaped lineage diversification in *Petrocoptis*.

2. Materials and methods

2.1. Plant material

According to the current taxonomic treatment in *Flora iberica* proposed by Montserrat & Fernández-Casas (Montserrat and Fernández-Casas, 1990), the genus *Petrocoptis* comprises nine species and three subspecies. For the purposes of our phylogenomic and morphometric analyses, and to ensure consistency in sampling design and data interpretation, we treated all eleven taxa as independent operational taxonomic units (OTUs) throughout this manuscript, as follows: *Petrocoptis crassifolia* Rouy, *P. glaucifolia* (Lag.) Boiss., *P. grandiflora* Rothm., *P. guarensis* Fern. Casas, *P. hispanica* (Willk.) Pau, *P. montserratii* Fern. Casas, *P. montsicciana* O.Bolòs & Rivas Mart., *P. pardoi* Pau, *P. pseudoviscosa* Fern. Casas, *P. pyrenaica* (Bergeret) A. Braun ex Walp. and *P. viscosa* Rothm.

A total of 63 distinct populations were sampled across the entire geographic range of *Petrocoptis* representing the full taxonomic diversity of the genus, as well as most of its morphological variation, and altitudinal and climatic gradients (Fig. 1a). Complete voucher information is provided in Supporting Information Table S1. Voucher specimens were deposited in the herbarium of the Pyrenean Institute of Ecology-CSIC (JACA, herbarium codes following standard abbreviations from Holmgren et al., 1990; and Thiers, 2024). Young leaf material was collected in the field and preserved in silica gel for subsequent genomic analyses (Table S1).

2.2. Seed morphometric measurements

Seed morphometric analyses were conducted on 58 of the 63 populations sampled. Five populations did not have mature individuals with seeds at the time of collection, nor were seeds present in previously collected herbarium materials from the same localities. For each population, a minimum of three individuals bearing mature, dehiscent capsules were randomly selected; sampling was extended up to ten individuals when fruit availability allowed it. For underrepresented populations, sampling was complemented with herbarium material from BIO, JACA, LEB, MA, SALA, SANT, VAL and VIT (Table S1). In total, 395 individuals were included, yielding 2097 seeds for analysis.

Digital images were acquired using a Leica MC190 camera mounted on a Nikon SMZ800 stereo microscope at 10× magnification and a resolution of 171 pixels mm^{-1}. Image processing was conducted semi-automatically using Leica Application Suite v4.12.0. Seed and strophiole diameters were measured manually, while seed area and strophiole relative size were automatically computed. Strophiolar hair morphology was also included in the dataset as a qualitative trait, categorized as cylindrical or claviform depending on apex width ($<$ or $>$50 μm, respectively), following Mayol and Rosselló (1999). A third character state combined category (for practical reasons hereafter called "mixed") was used when both hair types co-occurred within the same seed.

2.3. Floral trait measurements

Calyx length at anthesis was measured on 60 of the 63 populations sampled (Table S1), using a Mitutoyo 500-161U digital caliper. Three populations remained unrepresented due to insufficient herbarium material. In total, 1691 flowers of 377 individuals were measured. Petal colour was recorded as a binary qualitative trait, scored as either chromatic (pink) or achromatic (white) based on field observations.

2.4. DNA extraction, sequencing and assembly

A total of 15–20 mg of silica-dried leaf tissue per sample was homogenized and total genomic DNA was extracted using a 2× cetyltrimethylammonium bromide (CTAB) protocol following Csiba and Powell (2006). DNA was resuspended in 50 μL of Tris–EDTA (TE) buffer and deposited in the Plant DNA Biobank of the University of Salamanca (collection SALA-DNA, https://www.gbif.org/es/dataset/fe44aa08-0231-46d6-94d9-270673c5aedb). DNA concentration was quantified using a Qubit™ 4 Fluorometer (Thermo Fisher Scientific Inc., Waltham, MA, USA). Whole-genome shotgun libraries were prepared in half-volume reactions using the NEBNext Ultra II DNA Library Prep Kit for Illumina (New England Biolabs, Ipswich, MA, USA), starting from 250 ng of input DNA per sample. DNA was fragmented using the NEBNext Ultra II FS enzyme mix, which performs fragmentation, end repair, and dA-tailing. Libraries were size-selected with Sera-Mag Select Beads (Cytiva Life Sciences, Marlborough, MA, USA) to obtain fragments of approximately 150 bp and amplified with 12 PCR cycles using NEBNext Dual Index Primers Set 1. Library concentration was measured with Qubit, and fragment size distribution was assessed for a subset of samples using a TapeStation system (Agilent Technologies, Santa Clara, CA, USA). Equimolar amounts of individual libraries were pooled into

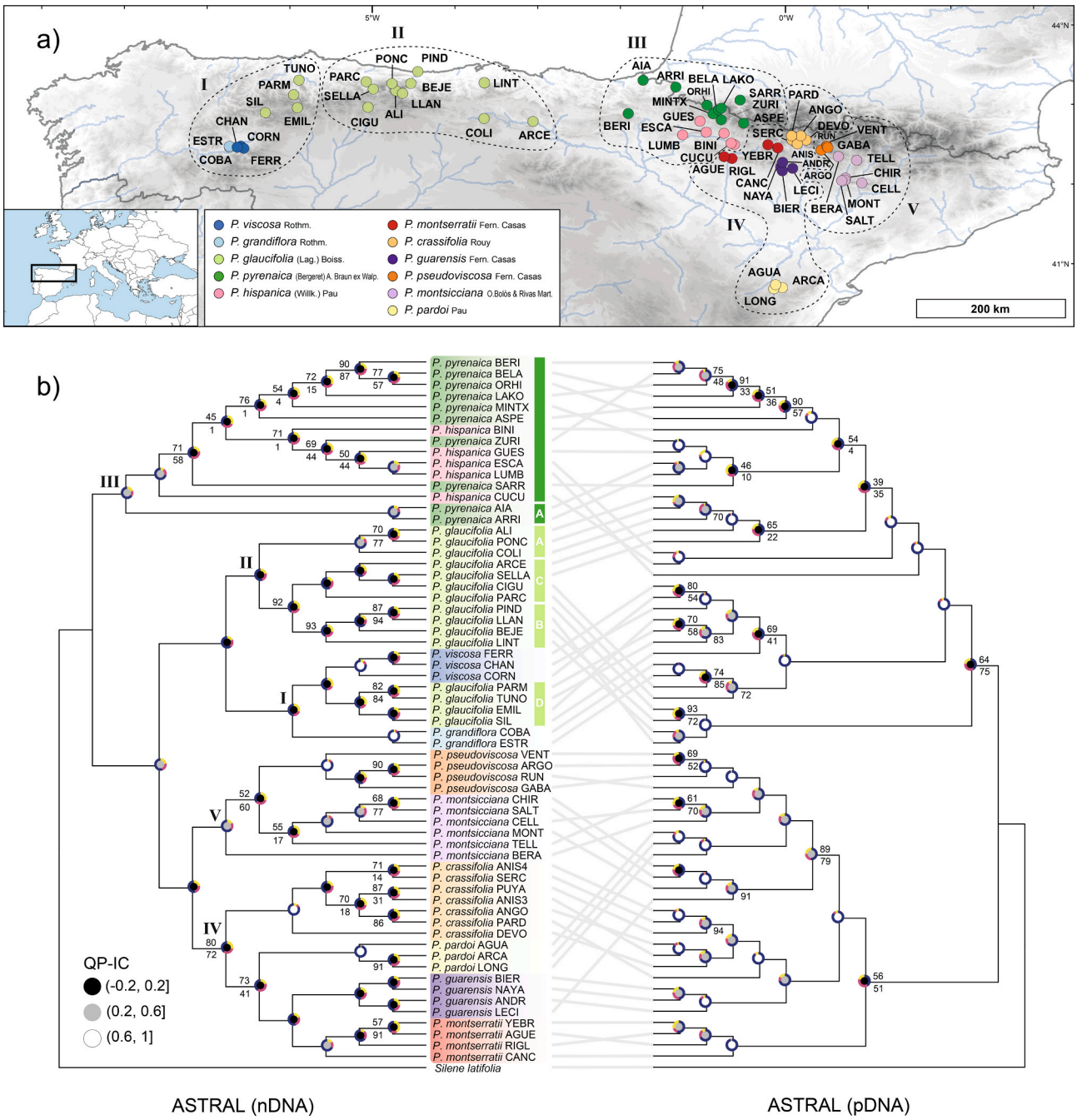

Fig. 1. a) Distribution of *Petrocoptis* sampled populations. OTUs are colour-coded for illustrative purposes. Populations from major clades are circumscribed in dashed lines: I: western Cantabrian range clade, II: central-eastern Cantabrian range clade, III: western Pyrenean range clade, IV: central Pyrenean and Iberian ranges clade, V: eastern Pyrenean range clade. b) Phylogenies of *Petrocoptis* nuclear (left) and plastid (right) datasets inferred using ASTRAL-III. Numbers above internal branches show ASTRAL-III local posterior probability (LPP). Number(s) below show bootstrap (BS) values and SH-like approximate likelihood ratio test (SH-aLRT) values, in the case of IQ-TREE. All unlabeled internal branches received full support (>95%). Coloured pie charts depict local posterior probabilities for the main topology (blue), the first alternative (red), and the second alternative (yellow). Greyscale dots in the center of the nodes indicate the quadripartition internode certainty (QP-IC) score. Major clades I-V are indicated in crown nodes. Population codes follow Supplementary Data Table S1.

thirteen enrichment pools prior to target capture. Hybridization-based enrichment was performed using the Angiosperms353 probe set (Johnson et al., 2019) in half-volume reactions at 60 °C for 20 hours, following the manufacturer's protocol (myBaits Expert Angiosperms-353, Arbor Biosciences, Ann Arbor, MI, USA). Post-hybridization library quality and fragment size distribution were assessed using a TapeStation system (Agilent Technologies, Santa Clara, CA, USA). Enriched pools were sequenced on a HiSeq platform (Illumina, Inc.) by Macrogen (Seoul, South Korea), generating 150 bp paired-end reads. Library preparation and hybridization were performed at the Plant DNA Biobank of the University of Salamanca (https://nucleus.usal.es/en/herbarium).

2.5. Sequence processing and locus recovery

Raw read quality was assessed using FastQC (Andrews, 2014) and summarized with MultiQC (Ewels et al., 2016). Adapter trimming and quality filtering were conducted with Trimmomatic v0.39 (Bolger et al.,

2014), using the following parameters: removal of low-quality bases at the 5′ and 3′ ends of reads (LEADING:30; TRAILING:30), exclusion of reads shorter than 60 bp (MINLEN:60), and application of a 4-bp sliding window filter to remove reads with average quality scores below 15 (SLIDINGWINDOW:4:15).

Filtered paired-end reads were processed with HybPiper v2.1.6 (Johnson et al., 2016) to retrieve nuclear loci targeted by the Angiosperms353 probe set, using the "mega353" target file (McLay et al., 2021). Reads were aligned to reference targets using BWA v0.7.18 (Li and Durbin, 2009), followed by *de novo* assembly with SPAdes v3.15.4 (Bankevich et al., 2012). Supercontigs (exons+introns) were extracted using Exonerate v2.4.0 (Slater and Birney, 2005). Loci flagged as paralogous by the paralog_retriever script were excluded from subsequent analyses. *Silene latifolia* Poir. was selected as outgroup and Angiosperms353 sequences were retrieved (GenBank: ERS1829296) from the One Thousand Plant (OneKP) Initiative (Leebens-Mack et al., 2019; Matasci et al., 2014).

For plastid analyses, all coding and intergenic regions from the *S. latifolia* plastome (GenBank: NC_016730; Sloan et al., 2012) were retrieved and redundant regions were removed resulting in a reference set of 217 non-overlapping plastid fragments. These were recovered from the *Petrocoptis* samples using HybPiper, as described above.

In total, 170 individuals yielded satisfactory nuclear locus recovery, although plastid sequencing success was uneven across samples. To ensure robust and comparable phylogenetic inference, a single representative individual per population (63 populations in total) was selected based on combined nuclear and plastid recovery metrics (see next section). All 170 individuals were retained for downstream analyses of nuclear genetic diversity (see final section of Materials and Methods).

All bioinformatic analyses were conducted on the high-performance computing infrastructure of Supercomputación de Castilla y León (SCAYLE; https://www.scayle.es).

2.6. Phylogenetic analysis

All loci were aligned with MAFFT v7.520 (Katoh and Standley, 2013) using the '-auto' option. Alignments were trimmed using TrimAl v1.4.15 (Capella-Gutiérrez et al., 2009) with the '-automated1' heuristic, which is optimized for downstream maximum likelihood (ML) analyses. Summary statistics for each alignment before and after trimming were calculated with AMAS (Borowiec, 2016) as a quality control step.

Both concatenation and coalescent-based approaches were used to infer species phylogenetic relationships. For concatenated analyses, nuclear and plastid partitioned supermatrices were assembled using FASconCAT-G v1.05.1 (Kück and Longo, 2014). ML phylogenetic inference was conducted in IQ-TREE v2.3.5 (Minh et al., 2020; Nguyen et al., 2015). The best fitting substitution model was selected using ModelFinder (Kalyaanamoorthy et al., 2017). An edge-proportional partition model was implemented using the -p option (Chernomor et al., 2016), allowing each partition to have independent evolutionary rates and proportional branch lengths. Node support was assessed using 1000 standard bootstrap replicates and 1000 SH-like approximate likelihood ratio test replicates (SH-aLRT; Guindon et al., 2010).

For coalescent-based phylogenetic analyses, individual gene trees were inferred separately for each nuclear locus using IQ-TREE with locus-specific substitution models. Support values were based on 1000 bootstrap replicates. Following Zhang et al., 2017, branches with bootstrap support (BS) below 30% were collapsed to reduce the impact of poorly supported relationships on downstream analyses.

Species trees were reconstructed under the multispecies coalescent framework using two complementary approaches: ASTRAL-III v5.7.8 (Zhang et al., 2018) and SVDquartets (Chifman and Kubatko, 2014), as implemented in PAUP* v4.0a169 (Swofford, 2003). In ASTRAL-III, the set of best ML gene trees was used as input and multilocus BS support was estimated using 200 gene tree bootstrap replicates with the "–i –b –r" options. Local posterior probabilities (LPP) were calculated for the main topology and quartet support values were obtained for the main topology (LR|SO), as well as for the first (RS|LO) and second alternative topologies (RO|LS). For SVDquartets the concatenated alignment was used, all possible quartets were evaluated, and node support was estimated from 200 bootstrap replicates. Quartet support values and LPP were also calculated for topologies derived from SVDquartets and concatenation-based analyses using the '-q' option in ASTRAL-III to allow direct comparison among methods.

2.7. Concordance analysis

To quantify the degree of genealogical conflict among loci, the quadripartition internode certainty metric QP-IC was calculated using QuartetScores (Zhou et al., 2020). This measure assesses the support for a given internal branch of a reference species tree across a collection of gene trees and provides an estimate of the extent to which alternative topologies are represented among loci. Prior to the analysis, gene tree branches with BS values below 50% were collapsed to reduce the influence of poorly supported relationships. Quadripartition internode certainty values were computed for species trees inferred using ASTRAL III, SVDquartets and concatenation-based approaches allowing direct comparison of concordance patterns across inference methods.

2.8. Unravelling Cytonuclear and Genealogical Conflicts

To evaluate whether the cytonuclear discordance observed at deep nodes could be explained by ILS alone or whether reticulate evolution also contributed to the observed patterns, two complementary approaches were implemented.

First, coalescent simulations under the multispecies coalescent (MSC) model were performed, following (Folk et al., 2017). A total of 10,000 plastid gene trees were simulated using DendroPy v5.0.6 (Moreno et al., 2024), with the nuclear species tree inferred with ASTRAL-III serving as the model topology. To account for haploid inheritance and reduced effective population size of plastid genomes, all branch lengths of the nuclear species tree were scaled by a factor of four (Folk et al., 2017; Morales-Briones et al., 2018; Yang et al., 2023a). Frequencies of bipartitions from the simulated plastid trees were then mapped onto the empirical plastome topology using RAxML v8.2.12 (Stamatakis, 2014). Under a scenario dominated by ILS, relationships shown in the empirical plastid tree should be present in the simulated plastid trees with high frequency. Conversely, under scenarios of reticulate evolution, unique clades in the empirical plastid tree should be absent in the simulated plastid trees, or detected at a low frequency (García et al., 2017).

Second, the fit of nuclear gene trees to the MSC model was evaluated using the quartet concordance framework developed by Allman et al., 2022. For each of the 345 nuclear loci, quartet count concordance factors (qcCFs) were computed using the quartetTreeTestInd function implemented in the R package MSCquartets (Rhodes et al., 2021), using R v4.4.2 (R Core Team, 2025). Simplex plots were generated under two alternative models, one assuming a known species tree (T1; using the ASTRAL-III topology) and another without a predefined species tree (T3). Under the MSC model, qcCFs should cluster along specific lines in the simplex plot; significant deviations suggest either substantial gene tree estimation error (GTEE) or biological processes beyond ILS, such as reticulate evolution. To further distinguish between these alternatives, quartets that significantly deviated from the MSC expectations (P value < 0.05) were mapped back onto the species tree. A non-random clustering of rejected quartets at particular nodes is indicative of localized reticulation whereas a random distribution is more consistent with stochastic error in gene tree inference.

Additionally, the extent of ILS along the species tree was quantified by estimating the parameter θ (theta), which reflects the relative contribution of ancestral polymorphism on gene tree discordance (Cai

et al., 2021). Theta was calculated by dividing branch lengths in mutation units estimated in IQ-TREE by the corresponding branch lengths in coalescent units inferred with ASTRAL-III. This metric provides edge-specific insights into the expected discordance attributable to ILS under the MSC framework.

2.9. Species network analysis

To explicitly test for the presence of reticulate evolutionary processes, phylogenetic, networks were inferred from the set of 345 nuclear gene trees using a maximum pseudo-likelihood approach implemented in PhyloNet v.3.8.2 (Than et al., 2008; Wen et al., 2018; Yu and Nakhleh, 2015). Prior to network inference, gene tree branches with bootstrap support values below 30% were collapsed to reduce topological uncertainty, following the recommendations of Mirarab's team for coalescent-based species tree inference, which suggest that moderate collapsing thresholds (10–33%) minimize species tree estimation errors while preserving informative gene tree discordance (Zhang et al., 2018). To limit computational complexity and focus on deeper evolutionary patterns, samples belonging to monophyletic clades were grouped using the -a taxa map option in PhyloNet.

Network searches were conducted permitting between zero and four reticulation events. Candidate networks were subsequently ranked according to their log pseudo-likelihood values, in accordance with the recommendation that pseudo-likelihood scores are not appropriate for conventional model comparison (Yu and Nakhleh, 2015) inferred using the Network inference Algorithm via NeighbourNet Using Quartets (NANUQ) method (Allman et al., 2019). This analysis relied on empirical quartet concordance data extracted from the gene trees and employed the NANUQ function within the MSCquartets R package, applying $\alpha = 0.05$ and $\beta = 0.95$ as confidence thresholds. Finally, to facilitate visualization, a split graph was generated using the NeighborNet algorithm as implemented in SplitsTree v6.4.17 (Huson and Bryant, 2024), based on quartet distances among taxa.

2.10. Evolution of seed and flower traits

2.10.1. Data preparation

Quantitative traits included in this section are: seed area, strophiole area, the ratio between strophiole and seed area, and calyx length for which population mean and standard error were calculated. Discrete traits included strophiolar hair type (classified as cylindrical, claviform or mixed) and petal colour (white or pink).

Climatic variables of annual precipitation and annual maximum temperature were extracted for each population using GIS tools (ArcMap v10.8, ESRI, 2020), from the Climatic Digital Atlas of the Iberian Peninsula (Ninyerola et al., 2005), with a spatial resolution of 200 m.

To obtain an ultrametric species tree with branch lengths proportional to mutation units IQ-TREE was run with the concatenated partition matrix with the ASTRAL-III nuclear species tree topology constraint (-g option).

2.10.2. Phylogenetic signal analyses

Pagel's λ (Pagel, 1999) and Blomberg's K (Blomberg et al., 2003) were estimated as two complementary metrics of phylogenetic signal, to assess the extent to which morphological variation is structured by evolutionary history. Both were calculated using the phylosig function in phytools R package (Revell, 2012, 2024), incorporating standard errors to account for within-species measurement uncertainty.

2.10.3. Ancestral character state reconstruction

To infer the evolutionary history of seed and flower morphological traits, the ancestral states for all four continuous traits under a Brownian motion model was reconstructed using the phytools fastAnc function. To account for measurement error and uncertainty, 1,000 trait datasets per variable were simulated from observed tip means and standard errors normal distributions. Each simulated dataset was used to estimate ancestral values, and the resulting distributions were summarised to obtain node-wise posterior means and 95% confidence intervals (CIs).

The evolution of strophiolar hair type was explored as a three-state discrete character (cylindrical, claviform and mixed). Maximum likelihood model-fitting approaches (fitMk function, phytools R package) was used to compare alternative models of state transitions: Equal Rates (ER), Symmetrical (SYM), All-Rates-Different (ARD), three ordered bidirectional models and six directional ordered models. The evolution of binary character petal colour was evaluated under ER, ARD, and two directional models (white → pink, and pink → white). Model support was assessed via Akaike Information Criterion (AIC, Sakamoto et al. 1986), and the best-fitting models were used to simulate stochastic character maps (make.simmap; Huelsenbeck et al. 2003).

For the discrete traits a total of 1,000 stochastic maps were generated under a Bayesian framework with transition rates drawn from the posterior distribution estimated by the best model. Posterior probabilities of ancestral states at each node were computed and visualised using the summary.simmap function (phytools R package) and corresponding plotting tools. This approach allowed detecting potential shifts in ecological strategies along the phylogeny in a probabilistic framework. Posterior probabilities of state transitions and node reconstructions of petal colour were also summarized and visualized using densityMap function.

2.10.4. Trait–environment relationships

Linear models were used to evaluate associations between morphological traits and climatic variables. To account for shared ancestry, a Phylogenetically Independent Contrasts (PICs, Felsenstein 1985) was performed using the pic function in ape R package (Paradis and Schliep, 2019). Prior to analysis, seed and strophiole area were square-root transformed.

2.10.5. Evolutionary modelling and bayesian shift detection

To model potential shifts in adaptive regimes along the phylogeny, two complementary approaches were employed: a Bayesian reversible-jump MCMC analysis (rjMCMC, Green 1995) using bayou R package (Uyeda and Harmon, 2014), and maximum-likelihood model selection using mvMORPH R package (Clavel et al., 2015).

For the Bayesian framework, the bayou.makeMCMC function (bayou R package) was used to define priors for model space and parameters (σ^2, α, θ), and ran five million MCMC iterations. Prior selection allowed the number of shifts (k) to vary (Poisson with $\lambda = 10$, $k \leq 50$) and used a half-Cauchy distribution for α and σ^2. Adaptive optima (θ) were modelled with a normal distribution centered on the observed mean. Convergence and burn-in (30%) were assessed visually and through summary statistics. Regime shifts were interpreted with posterior probability (PP) > 0.5 as strongly supported shifts (Uyeda and Harmon, 2014).

To test whether shifts in seed and floral trait optima were associated with specific states of discrete characters, a range of evolutionary models were fitted using the mvMORPH package. In the case of seed morphology, a phylogenetic principal component analysis (phyl.pca function, phytools R package) was first performed to reduce the dimensionality of the dataset. The analysis included three standardized (mean = 0, SD = 1) variables: seed and strophiole area (both square-root transformed to improve normality), and strophiole relative size (untransformed). The second principal component axis (PC2), which captured opposing variation in seed size and strophiole relative size, was used in subsequent comparative analyses. For floral morphology, we used the raw measurement of calyx length as a continuous trait. Trait optima (θ), evolutionary rates (σ^2), and selection strengths (α) were estimated under four model classes: i) single-rate Brownian motion (BM1), ii) multiple-rate Brownian motion (BMS), iii) single-optimum Ornstein–Uhlenbeck (OU1), and iv) multi-optima OU (OUM). Simulated regime histories were drawn from 1,000 stochastic character maps

of strophiolar hair type and petal colour, each generated under the corresponding best-fitting evolutionary model (see "Ancestral State Reconstruction" section). Each regime map was used to fit the model to the respective continuous trait. Model comparison and selection was based on Akaike Information Criterion (AIC and AICc). Estimated parameters were used to identify adaptive optima associated with discrete character states.

2.10.6. SNP extraction, genetic diversity, and phylogenetically informed trait associations

To identify loci polymorphisms, raw paired-end reads were aligned to a reference composed of the best supercontigs of all "mega353" loci using BWA-MEM v0.7.17 (Li, 2013). BAM files were sorted and indexed with SAMtools v1.17 (Li et al., 2009), and read groups were added with GATK v4.4.0.0 (McKenna et al., 2010). PCR duplicates were marked, and individual Genomic Variant Call Format files (GVCFs) were generated using GATK HaplotypeCaller in GVCF mode (Poplin et al., 2018).

Per-sample GVCFs were aggregated with GATK CombineGVCFs, followed by joint genotyping using GenotypeGVCFs. Hard filters were applied to remove low-quality variants based on standard metrics: quality by depth (QD < 5.0), strand bias (FS > 60.0), mapping quality (MQ < 40.0), and read position and mapping quality rank sums (ReadPosRankSum < -8.0; MQRankSum < -12.5), following GATK Best Practices recommendations (Depristo et al., 2011; Slimp et al., 2021; Van der Auwera and O'Connor, 2020). Only biallelic SNPs passing all filters were retained in the final VCF file.

Variant data were processed in PLINK v1.9 (Purcell et al., 2007) to obtain filtered independent SNPs. Missingness thresholds were set at 30% per SNP and per individual, minor allele frequency was filtered at 5%, and linkage disequilibrium (LD) pruning was performed (window size = 400 SNPs, step = 10 SNPs, r^2 threshold = 0.5) to reduce correlations among loci. Following these filters, 4.266 variants and 170 individuals representing all the 60 represented populations with flower measurements passed quality controls and were retained for downstream analyses.

Individuals were grouped attending the distinct genetic lineages identified in this work (see Results section). Poorly represented groups were merged with closely related ones to achieve more balanced sample sizes (*Petrocoptis glaucifolia* clade D + *P. viscosa*, and *P. pyrenaica* + *P. hispanica*), preserving phylogenetic coherence.

Classical measures of expected (He) and observed heterozygosity (Ho) were not estimated at the lineage level because samples belong to different populations with potentially distinct allele frequency distributions, violating the assumptions of panmixia required for meaningful within-lineage estimates. Instead, we implemented a lineage-level proxy for genomic diversity based on the relative prevalence of highly heterozygous loci. This approach avoids biases associated with unequal sample sizes and slight differences in recovered alignment length among the 13 genetic lineages.

Specifically, we quantified the number of highly heterozygous SNPs (HH-SNP) per lineage. From the PLINK genotype matrix, a SNP × individual allele-dosage table was generated and individuals were grouped according to the genetic lineages identified in this study. For each SNP within each lineage, we calculated the proportion of individuals that were heterozygous (i.e. number of heterozygous individuals divided by total individuals sampled in that lineage). A SNP was classified as highly heterozygous when the frequency of heterozygous genotypes within a lineage was ≥0.75.

The 0.75 threshold corresponds to the theoretical maximum heterozygosity expected under Hardy–Weinberg equilibrium in a system with four equally frequent alleles (H = 0.75 when p = 0.25 for each allele). Because most SNPs are rarely tetrallelic in practice, this criterion is highly conservative and identifies loci exhibiting exceptionally high heterozygosity relative to neutral expectations.

The HH-SNP metric was therefore defined as the total number of SNPs per lineage with heterozygosity frequency ≥75%, providing a standardized proxy for lineage-level genomic diversity.

To examine the influence of HH-SNPs on floral traits while accounting for shared ancestry, phylogenetic mixed models were implemented using the R package MCMCglmm (Hadfield, 2010). Two response variables were modelled: calyx length (continuous) and petal colour (binary: pink/white). Standardized HH-SNP was considered as predictor variable. Phylogenetic non-independence was incorporated via the inverse of the phylogenetic covariance matrix derived from the reference ASTRAL-III species tree. Gaussian priors ($V = 1$, $n = 1$, $\nu = 1$) were applied for calyx length models, and categorical priors ($V = 10$, $n = 1$, $\nu = 10$) for petal colour models (Hadfield, 2010).

Three independent MCMC chains per model (Gaussian: number of MCMC iterations = 1.25e6, burnin = 2.5e5, thinning interval = 100; categorical: number of MCMC iterations = 6e7, burnin = 1e7, thinning interval = 500) were ran. Convergence was assessed via Heidelberger-Welch's diagnostics (Heidelberger and Welch, 1981), effective sample size, and autocorrelation. Posterior distributions of SNP effects on calyx length and petal colour were summarized using highest posterior density intervals (HPD 95%). Phylogenetic heritability (H^2) was estimated as the proportion of total variance attributable to phylogenetic structure for both traits (Hadfield, 2010).

Posterior predictions were generated across the observed range of HH-SNPs to visualize the expected relationship between clade-level genetic diversity and trait variation. These predictions allowed the estimation of changes in calyx length and the probability of pink petals as a function of HH-SNP, highlighting potential links between genomic diversity and floral evolution.

3. Results

3.1. Sequence recovery and alignment metrics

Target enrichment using the Angiosperms353 probe set yielded high recovery success across all sampled individuals of *Petrocoptis*. After read trimming and quality filtering, 345 nuclear low-copy supercontigs were retained for phylogenomic analyses (Table S2). Loci flagged as paralogous by the HybPiper pipeline were excluded to ensure orthology. The mean gene recovery rate across samples was 54.75 ± 22.32%, with an average of 200 ± 72 loci recovered at ≥50% of the target length.

Preliminary analyses using alternative locus recovery thresholds yielded highly consistent topologies, suggesting that moderate levels of missing data did not substantially affect phylogenetic inference, in agreement with previous phylogenomic studies (Molloy and Warnow, 2018).

For plastid analyses, 192 non-overlapping coding and intergenic regions were successfully retrieved (Table S3). Plastid gene mean recovery rate across selected samples was 89.45 ± 15.09%, with an average of 183 ± 16 regions recovered at ≥50% of their target length.

After aligning and trimming, the resulting concatenated nuclear matrix had a length of 243060 bp with 16904 parsimony-informative sites, whereas the plastid matrix had an aligned length of 121659 bp with 3944 parsimony-informative sites. Alignment and matrix statistics (Tables S4–S7), showed consistent representation across all taxa sampled OTUs, minimizing missing data and reducing stochastic noise in tree estimation.

3.2. Phylogenetic relationships

Coalescence and concatenated species trees were highly congruent at deep nodes for the nuclear dataset (Fig. S1). Most of the major clades and relationships among them were well supported (BS, SH-aLRT and LPP ≥ 95). Among all the predefined reference OTUs, *Petrocoptis pyrenaica*, *P. hispanica* and *P. glaucifolia* appeared as the most incongruent ones. Accordingly, we redefined some monophyletic groups within these lineages to ease further analysis and discussions (i.e. *P. pyrenaica* A and *P. glaucifolia* A, B, C and D, Fig. 1b).

Most reference OTUs were consistently recovered as monophyletic with high support, except for *Petrocoptis hispanica* which showed tips intercalated across *P. pyrenaica*. However, the two westernmost populations of *P. pyrenaica* (*P. pyrenaica* A), consistently appeared in all phylogenetic trees as a sister group to the rest of the *P. pyrenaica* and *P. hispanica* complex, together defining the western Pyrenean range clade (clade III; Fig. 1a, b). Similarly, *P. pseudoviscosa* was consistently nested within *P. montsicciana*, both constituting the eastern Pyrenean range clade (clade V; Fig. 1a, b).

The reference OTU *Petrocoptis glaucifolia* was recovered as polyphyletic. Populations from the central-eastern Cantabrian Mountains clustered in a well-supported lineage including *P. glaucifolia* A, B and C, corresponding to the central-eastern Cantabrian Mountains clade (clade II; Fig. 1a, b). In contrast, populations from the western Cantabrian Mountains (*P. glaucifolia* D) formed a distinct monophyletic lineage sister to *P. viscosa* and, together with *P. grandiflora*, constituted the western Cantabrian Mountains clade (clade I; Fig. 1a, b).

Petrocoptis crassifolia, P. guarensis, P. montserratii and *P. pardoi* each formed well-supported monophyletic lineages that together defined the central Pyrenean and Iberian ranges clade (clade IV; Fig. 1a, b), although the placement of *P. pardoi* received only moderate support (73 LPP; 41% BS). Despite minor discordances at shallow nodes, the strong congruence among nuclear inference methods supported the use of the ASTRAL coalescent tree for subsequent analyses.

Interestingly, the QP-IC scores of Quartet Scores concordance analysis were low for most clades, suggesting a high degree of conflict among nuclear gene trees (Fig. 1b). Deep branches displayed low to negative QP-IC values, indicating considerable support for alternative topologies among loci. In contrast, tipward nodes corresponding to monophyletic taxa consistently exhibited high QP-IC scores, suggesting stronger gene tree concordance at recent divergence events. This pattern is consistent with the expectation that ILS and potential reticulation disproportionately affect deeper phylogenetic relationships.

The plastid ASTRAL phylogeny was internally well supported (BS > 95%) and topologically stable across analyses (Fig. S2), yet displayed substantial topological incongruence with the nuclear tree (Fig. 1b). Several clades supported in nuclear analyses were not recovered in the plastome topology. For instance, *Petrocoptis glaucifolia* B was recovered as sister to the western Pyrenean and Cantabrian range clades, whereas *P. montserratii* was recovered as sister to the clade made of central Pyrenean-Iberian ranges and eastern Pyrenean range. *P. glaucifolia* A and C were nested (with a few samples in a more external position) within the *P. pyrenaica-P. hispanica* complex, suggesting a shared plastid ancestry. The position of *P. pardoi* is also noteworthy, as it appeared in the plastid phylogeny embedded within the eastern Pyrenean range clade, together with *P. montsicciana* and *P. pseudoviscosa*. Most notably, the reference OTUs *P. montsicciana* and *P. guarensis*, monophyletic in the nuclear phylogeny, turned polyphyletic in the plastid one. Overall, the genus *Petrocoptis* displays a strong signal of cytonuclear discordance, potentially reflecting differing evolutionary histories between the nuclear and plastid genomes.

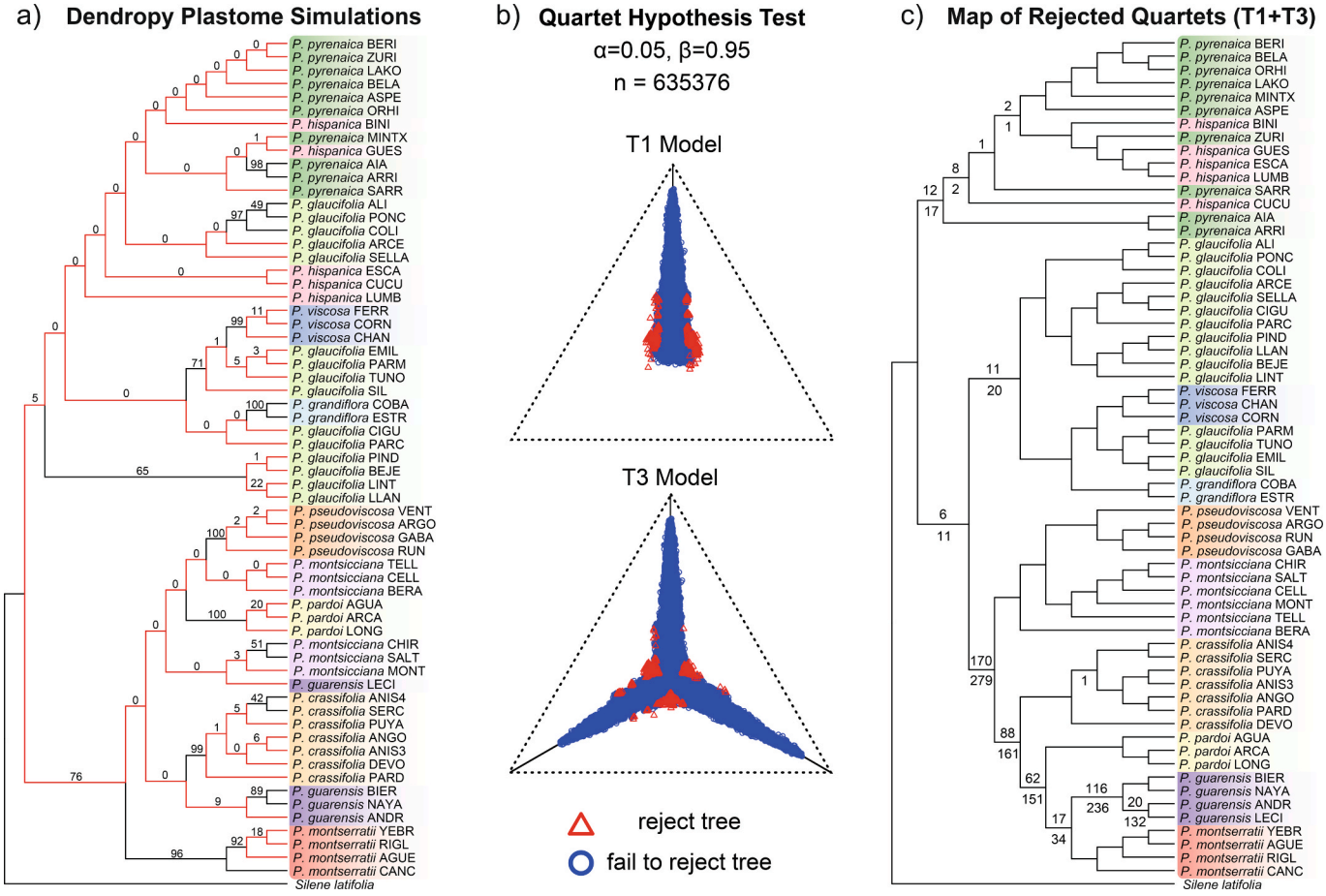

Fig. 2. Detecting the source(s) of cytonuclear and genealogical discordance. a) Summary of results of Dendropy plastome tree simulations. Red internal branches indicate clades unique to the plastid topology compared with the nuclear species tree. Numbers above internal branches show clade frequency (%) among simulated plastid genes. b) Simplex plots of quartet count concordance factors (qcCFs) for the 345 nuclear gene trees. c) Map of rejected quartets on nuclear phylogeny. Numbers above and below internal branches show the amount of quartets that reject the multispecies coalescent T1 and T3 models, respectively, in MSCquartets analyses. Population codes follow Supplementary Data Table S1.

3.3. Cytonuclear and Genealogical Discordance Analysis

The results of the coalescent simulation revealed that most clades present in the empirical plastid topology occurred at low frequencies among simulated plastome trees (below 22%), with the exception that 76% of simulated plastome trees agreed with the sister relationship between *Petrocoptis montserratii* and the rest of the central Pyrenean-Iberian ranges and eastern Pyrenean range clades (i.e., *P. crassifolia, P. guarensis, P. pardoi, P. montsicciana* and *P. pseudoviscosa;* Fig. 2a). Deep-level relationships, as well as clades corresponding to well-supported nuclear monophyletic groups, were particularly underrepresented, with recovery frequencies below 5%. These findings suggest that incomplete lineage sorting (ILS) alone cannot explain the cytonuclear discordance observed in *Petrocoptis*, pointing instead to additional processes, such as reticulate evolution, as likely contributors.

Quartet concordance factor (qcCF) statistics further supported a role for reticulation, in addition to ILS, in generating gene tree conflicts. T1 and T3 simplex plots showed that most empirical quartets were positioned close to the model expectation lines (Fig. 2b), but a subset deviated substantially. At the $\alpha = 0.05$ significance level, 0.10% (T1) and 0.19% (T3) of tests rejected the MSC hypothesis. Mapping these outlier quartets onto the species tree revealed clustering at several internal nodes (Fig. 2c), a pattern inconsistent with ILS alone and more indicative of localized reticulation. Nonetheless, the majority of qcCFs were located on or near the T1 and T3 model lines, with some clustered near the simplex centroids, consistent with an additional contribution of ILS to overall discordance.

Estimates of θ (theta) varied minimally across the species tree, ranging from 0.00 to 0.03 (Fig. S3). Despite these low θ values, several branches exhibited high levels of discordance, another evidence that ILS itself is not sufficient to account for the observed phylogenetic conflicts.

3.4. Phylogenetic network inference

Network analyses provide strong evidence that the diversification of *Petrocoptis* has been influenced by reticulate evolution. Among the candidate networks of the Phylonet analysis, the topology with two reticulation events exhibited the highest log pseudo-likelihood score (Fig. 3a; Table S8). Through the first reticulation event, *Petrocoptis pardoi* arose between an ancestor of *P. montsicciana-P. pseudoviscosa* clade and an ancestor of *P. guarensis,* with inheritance probabilities of $\gamma = 0.78$ and $\gamma = 0.22$, respectively. An additional reticulation event occurred between an ancestor of *P. glaucifolia* B clade ($\gamma = 0.85$) and an ancestor of *P. glaucifolia* D – *P. viscosa* ($\gamma = 0.15$), resulting in *P. glaucifolia* C clade.

The resulting level-1 network derived from NANUQ method using empirical quartet concordance data, supported the intricate reticulation that shaped the evolutionary history of *Petrocoptis pardoi* and provided additional resolution on population-level relationships (Fig. 3b).

3.5. Evolution of Continuous Seed and Flower Traits

Seed area, strophiole area, strophiole relative size, and calyx length exhibited significant phylogenetic signal (Fig. S4). Pagel's lambda was consistently high, with values of 1 for every trait, all of which were significantly different from zero ($p < 0.001$). Blomberg's K values were 2.18 for seed area, 1.21 for strophiole area, 1.05 for strophiole relative size and 2.12 for calyx length, and were also significant in all cases ($p = 0.001$), indicating moderate to strong phylogenetic structure.

Ancestral state reconstructions revealed directional trends in both seed and floral morphology across the phylogeny. In particular, changes in seed area (Fig. S5a) and calyx length (Fig. S5b) were associated with the divergence of specific clades, reflecting phylogenetically structured shifts in these traits. By contrast, variation in strophiole area (Fig. S6a) and strophiole relative size (Fig. S6b) appeared largely independent of deep phylogenetic structure, displaying heterogeneous patterns and transitions at the population level rather than consistent trends among clades.

Significant correlations were detected between strophiole traits and climatic variables using phylogenetic independent contrasts (Table S9). Strophiole area (square-root transformed) exhibited a positive association with maximum annual temperature ($F = 12.770$, $p = <0.001$, $R^2 = 0.171$; Fig. S6c) and a negative association with annual precipitation ($F = 5.641$, $p = 0.021$, $R^2 = 0.075$). Strophiole relative size also correlated

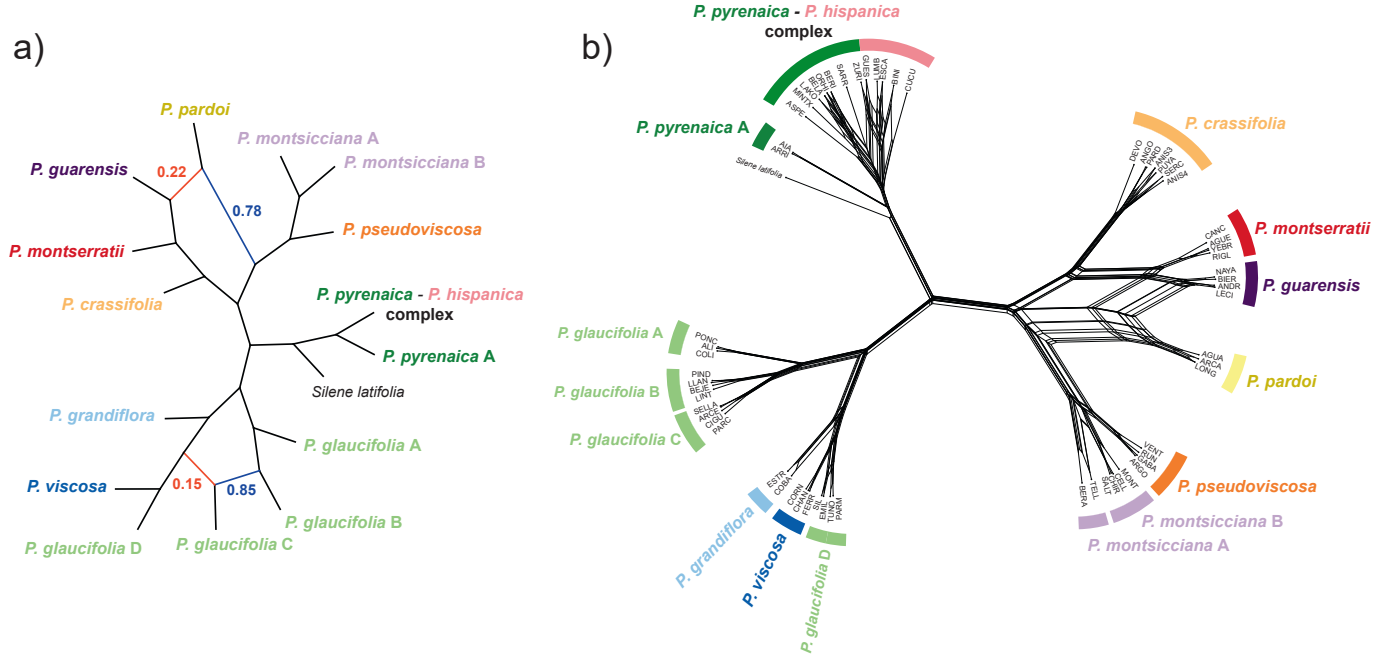

Fig. 3. a) Best species network inferred from PhyloNet based on pseudo-likelihood analyses. Blue and red lines indicate greater and lesser parental contributions, respectively, to hybrid lineages. Numbers adjacent to branches indicate inheritance probabilities for each hybrid node. b) Species network inferred by the NANUQ algorithm implemented in MSCquartets. Colours depict OTUs. Population codes follow Supplementary Data Table S1.

positively with maximum temperature ($F = 15.220$, $p = <0.001$, $R^2 = 0.200$; Fig. S6d) and negatively with precipitation ($F = 8.607$, $p = 0.005$, $R^2 = 0.118$). Seed area showed no evidence of significant correlation with any of the climatic variables considered (Table S9).

3.6. Evolution of Discrete Traits

The evolution of strophiolar hair type was best explained by an ordered, bidirectional model (ORD), which assumes directional transitions from cylindrical to claviform hairs via a mixed state (Fig. 4a). This model yielded the lowest AIC (58.312) and the highest Akaike weight (0.656), outperforming the rest of the models (Table S10). Stochastic character mapping under the ORD model (1,000 replicates) reconstructed a cylindrical-haired ancestor at the root of the phylogeny with full posterior support, and identified a transition towards mixed and claviform hairs in the central Pyrenean-Iberian ranges clade and eastern Pyrenean range clade (Fig. 4b), as well as a reversion to cylindrical hairs in the *Petrocoptis pseudoviscosa* clade.

In the case of petal colour, the equal-rates (ER) model was the best supported among the models tested (AIC = 63.114; Akaike weight = 0.334; Table S11), indicating similar rates of transition between white and pink states (Fig. 5a). However, both directional models—one favouring transitions from white to pink and the other from pink to white—showed comparatively low but non-negligible support (AIC = 63.230 and 63.973, respectively), suggesting the potential relevance of either directional selection in specific lineages. White corollas were consistently reconstructed as ancestral with high posterior probability (Fig. 5b, Fig. S5). Stochastic mapping supported six (HPD 95% = 2 – 10) independent gains of pink petals across all major clades (Fig. 5c) and two (HPD 95% = 1 – 9) likely reversals to white (Fig. 5d), especially conspicuous in *Petrocoptis montserratii* and *P. pseudoviscosa* clades.

3.7. Adaptive regime shifts in seed and flower traits

Bayesian reversible-jump modelling using bayou identified multiple shifts in the selective optima of both seed area and calyx length across the phylogeny, each with posterior probabilities exceeding 0.5. For seed area, the estimated optimum at the root corresponded to small seeds (1.227 ± 0.192 mm^2), with a selection rate (α) of 0.633 ± 0.560, indicating a moderate tendency for lineages to return toward their respective optima (θ). Six shifts in seed size optima were detected (Fig. 6a; Table S12), five of which occurred at the base of monophyletic clades identified in the phylogeny, and one at the population level (*Petrocoptis glaucifolia* PARM). Among the clade-level shifts, three represented increases in seed size optimum—at the base of the central Pyrenean-Iberian ranges and eastern Pyrenean range clade (from θ_1=1.227mm^2 to θ_2=2.132 mm^2), the *P. crassifolia* clade (from θ_1=2.132mm^2 to θ_2=2.617mm^2), and the *P. glaucifolia* B–*P. glaucifolia* C clade (from θ_1=1.227mm^2 to θ_2=1.327mm^2)—whereas two corresponded to reversions toward smaller seed size optima, at the bases of the *P. pseudoviscosa* clade (from θ_1=2.132mm^2 to θ_2=1.114mm^2) and *P. pardoi* clade (from θ_1=2.132mm^2 to θ_2=1.254mm^2).

For calyx length, the estimated optimum at the root corresponded to small flowers (7.530 ± 1.043 mm), with an α of 0.686 ± 0.378. Seven shifts in calyx length optima were detected (Fig. 6b; Table S13), six of which occurred at the base of previously identified monophyletic clades, and one at the population level (*Petrocoptis hispanica* BINI). All shifts indicated increases in calyx length, occurring at the base of the large central Pyrenean-Iberian ranges and eastern Pyrenean range clade (from θ_1=7.363 mm to θ_2=11.418 mm), the *P. crassifolia* clade (from θ_1=11.418 mm to θ_2=12.769 mm), the *P. guarensis* clade (from θ_1=11.418 mm to θ_2=14.062 mm), the *P. glaucifolia* B–*P. glaucifolia* C clade (from θ_1=7.363 mm to θ_2=8.726 mm), a subclade of *P. glaucifolia* D (from θ_1=7.363 mm to θ_2=9.317 mm), and the *P. grandiflora* clade (from θ_1=7.363 mm to θ_2=13.897 mm).

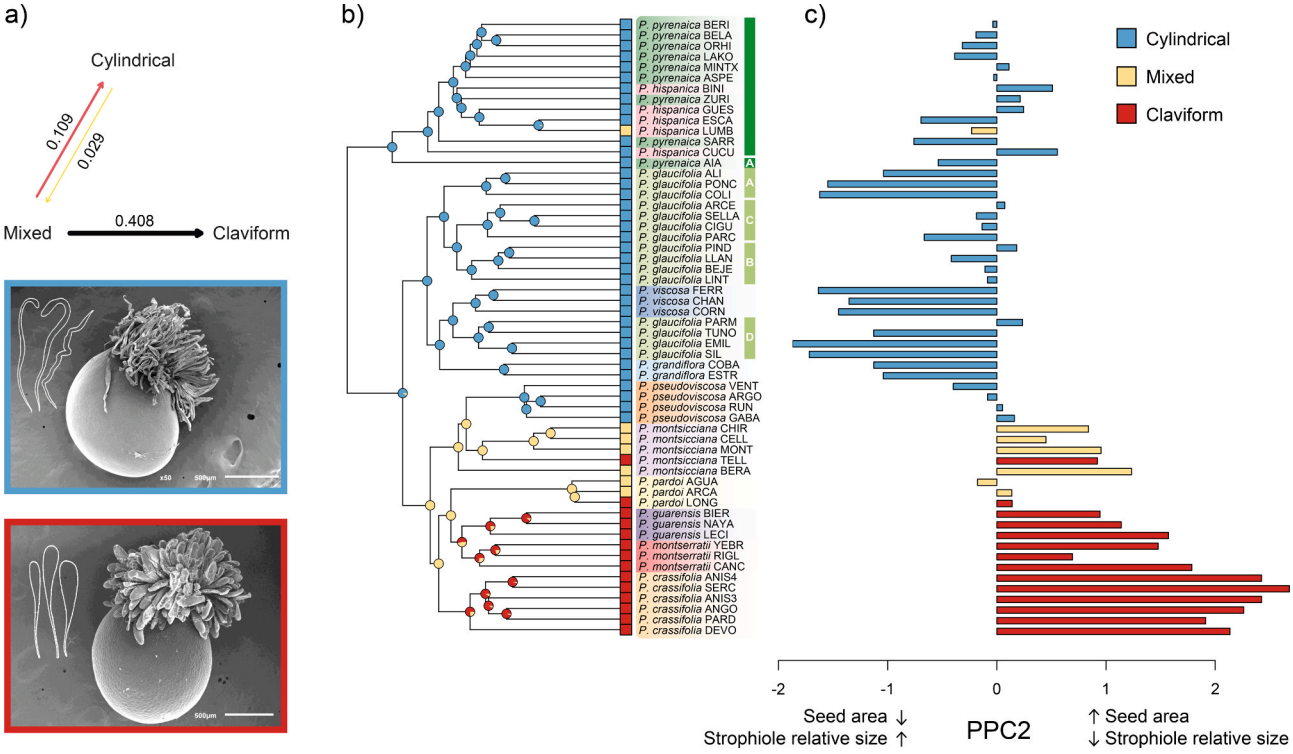

Fig. 4. a) Transition-rate (Q) matrix under the ordered model, illustrating the relative probability of state changes. b) Stochastic character mapping of strophiole hair type under the best-fitting ordered model. Posterior probabilities of states at internal nodes are indicated by coloured pies, and tip colours denote observed character states. c) Adaptive evolution of seed–strophiole covariation (PPC2) in *Petrocoptis* in relation to strophiolar hair morphology. Bars represent PPC2 scores and colours denote discrete hair morphologies. Population codes follow Supplementary Data Table S1.

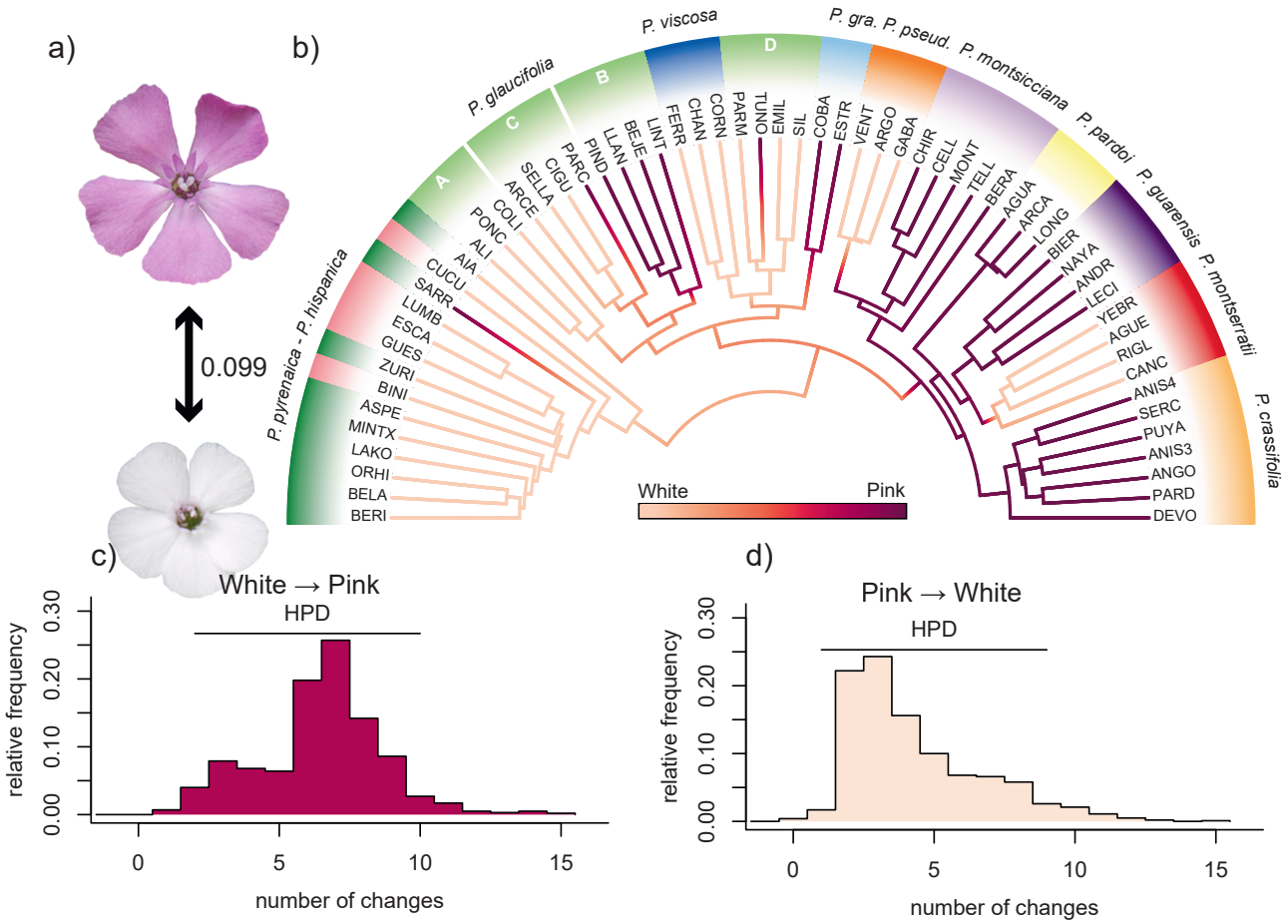

Fig. 5. Evolution of petal color in *Petrocoptis* based on stochastic character mapping. a) Transition-rate (Q) matrix under the equal-rates (ER) model, illustrating the relative probability of state changes of petal colour. b) Density map showing the reconstructed history of petal colour transitions under the ER model, with posterior probabilities of states displayed with branch colours ranging from purple (corresponding to pink flowers with a PP of 100%) to light pink (corresponding to white flowers with a PP of 100%). Population codes follow Supplementary Data Table S1. Colours at the tips depict prior taxonomic identification. c–d) Transition density plots summarizing the posterior distribution of changes between colour states across 1,000 simulations, with 95% Highest Posterior Density (HPD) interval: c) transitions from white to pink petals, and d) transitions from pink to white petals. OTUs full names: *P.gra. : P. grandiflora, P. pseud.: P. pseudoviscosa.*

Collectively, these results reveal a pattern of repeated, phylogenetically structured increases in calyx length, alongside with both increases and decreases in seed size, reflecting complex adaptive trajectories during the diversification of *Petrocoptis*.

To evaluate potential associations between continuous and discrete morphological character states, we fitted a set of evolutionary models to both seed and flower datasets. In the case of the second phylogenetic principal component (PPC2) of seed morphometric traits—positively associated with seed area and negatively associated with strophiole relative size—the OUM model provided the best fit (Table S14), indicating distinct morphometric optima (θ) for each strophiolar hair type under a single evolutionary rate (σ^2) and selection rate (α) across all regimes (Table S15). The highest PPC2 optimum, corresponding to large seeds with relatively small strophioles, was associated with claviform hairs (θ = 3.072), followed by mixed hairs (θ = 1.173). In contrast, the lowest optimum, indicative of small seeds with relatively large strophioles, was linked to cylindrical hairs (θ = –0.504). These results suggested that strophiolar hair morphology is functionally linked to coordinated changes in seed size and strophiole relative size.

Again, an OUM model, which outperformed the rest of models assessed the evolution of calyx length in relation to petal colour (Table S16), and estimated longer calyces in plants with pink corollas (θ = 11.91) compared with shorter calyces in white-flowered plants (θ = 7.83, Table S17).

Altogether, these results indicate a coordinated evolution of floral size and petal colour.

3.8. Associations between genetic diversity and floral traits across phylogenetic lineages

The number of highly heterozygous SNPs varied from 106 to 178 across the 60 sampled populations with recorded floral traits, representing distinct lineages (Fig. 7a). The studied floral traits exhibited strong phylogenetic structuring. Phylogenetic heritability (H^2) was 0.888 (0.769–0.972) for calyx length and 0.936 (0.876–0.988) for corolla colour. These values indicate that most of the variance in floral morphology is explained by shared ancestry, confirming the necessity of using phylogenetically informed models.

The Gaussian phylogenetic mixed model revealed a strong positive relationship between within-group genetic diversity and calyx length (posterior mean = 1.02, pMCMC = 0.0008; Fig. 7b, Table S18). Populations with higher heterozygosity tended to display longer calyces, a pattern consistent across major clades. The model showed no evidence of chain autocorrelation or non-convergence (Table S19). The random phylogenetic effect was substantial (posterior mean = 2.16, 95% HPD = 1.31–3.09), confirming strong phylogenetic structure, while residual variance was comparatively low (posterior mean = 0.27, 95% HPD = 0.07–0.55).

Similarly, the binomial phylogenetic model of petal colour showed that the probability of pink corollas increased markedly with genetic

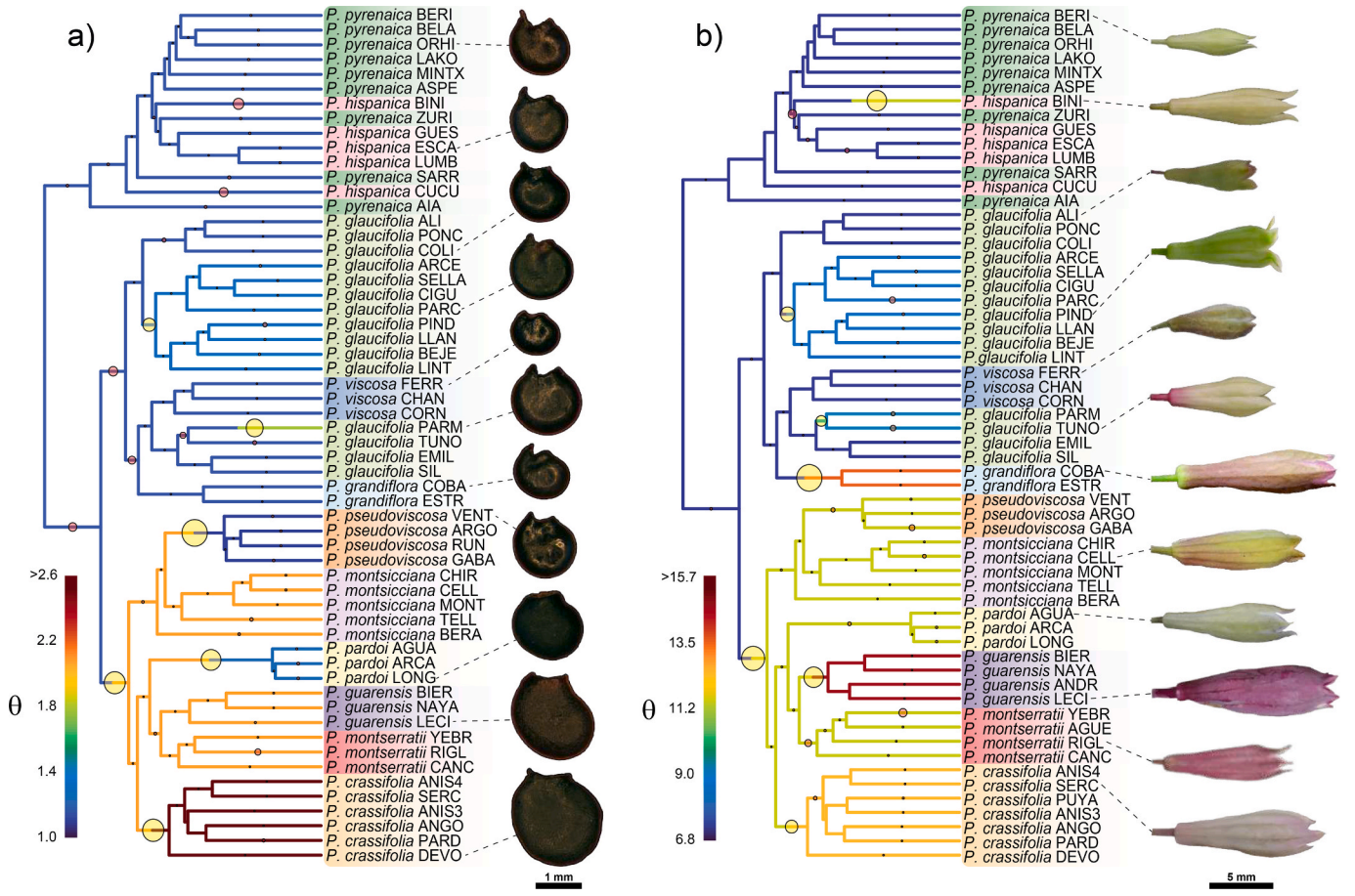

Fig. 6. Posterior mapping of adaptive regime shifts in seed area (a) and calyx length (b) along the phylogeny of the genus *Petrocoptis*. The diameter of the circles at the nodes is proportional to the posterior probability (PP) of a regime shift on the corresponding edge. Yellow circles depict shifts with PP > 0.5. All regimes with PP of a regime shift >0.5 are mapped using different colours, which are coded to display the mean value of θ for that edge from the posterior sample. Population codes follow Supplementary Data Table S1.

diversity (posterior mean = 5.91, pMCMC < 0.0001; Fig. 7c, Table S20). Lineages with greater counts of highly-heterozygous SNPs (HH-SNPs) were more likely to exhibit pink flowers rather than white ones. The categorical model achieved excellent convergence (Table S21). Phylogenetic variance was high (posterior mean = 19.73, 95% HPD = 4.54–44.81), reflecting strong phylogenetic dependence of floral colour.

Taken together, these results suggest that both calyx length and colour are positively associated with within-group genetic diversity. Lineages characterized by higher genomic heterozygosity (e.g., *Petrocoptis glaucifolia B*, *P. guarensis*, Fig. 7a) tend to bear pink flowers with longer calyces, whereas those with lower diversity (e.g., *P. pyrenaica-P. hispanica, P. pseudoviscosa*) produce white flowers with shorter calyces. This pattern remains significant after accounting for phylogenetic covariance.

4. Discussion

4.1. Evolutionary history and species relationships in the Iberian endemic chasmophytic genus Petrocoptis

Our phylogenomic analyses provide the most comprehensive reconstruction to date of evolutionary relationships within *Petrocoptis*, substantially refining earlier hypotheses based on a limited number of loci while also confirming pervasive genealogical conflict. Extensive incongruence among nuclear gene trees, as well as between nuclear and plastid genomes, emerges as a dominant feature in the evolution of the genus. Cytonuclear discordance is widely documented across angiosperms and is frequently interpreted as the genomic footprint of complex evolutionary histories involving ILS, hybridization and introgression (Cai et al., 2021; Morales-Briones et al., 2021; Morales-Briones et al., 2018; Yang et al., 2023a,b).

In *Petrocoptis*, however, several independent lines of evidence indicate that ILS alone cannot explain for the observed patterns. Our coalescent simulations show that most strongly supported plastid clades are recovered at extremely low frequencies under an ILS-only model (Fig. 2a). Quartet concordance analyses further reveal clusters of rejected quartets concentrated around specific nodes rather than randomly distributed across the phylogenetic tree (Fig. 2c). Together with the presence of short internodes and a poorly resolved backbone in the nuclear species tree, these results support a scenario of rapid diversification accompanied by reticulate evolution.

Rapid radiations are particularly prone to reticulation because lineage splitting can occur before strong reproductive barriers are fully established, rendering species boundaries temporarily permeable (Anderson and Stebbins, 1954; Mallet, 2007; Seehausen, 2013, 2004; Vargas et al., 2017). Under such conditions, ancestral polymorphisms may persist and gene flow among diverging lineages can be extensive, generating mosaic genomic patterns. The phylogenetic topology of *Petrocoptis*, with unresolved deep nodes but strong support for terminal clades, conforms to this expectation and mirrors patterns documented in other rapidly diversified plant groups inhabiting topographically complex regions such as *Calochortus* Pursh (Liliaceae, Dilley et al., 2000), *Vriesea* Lindl. (Bromeliaceae, Loiseau et al., 2021), *Rhododendron* L. (Ericaceae, Ma et al., 2022) or many others (Whitney et al., 2010).

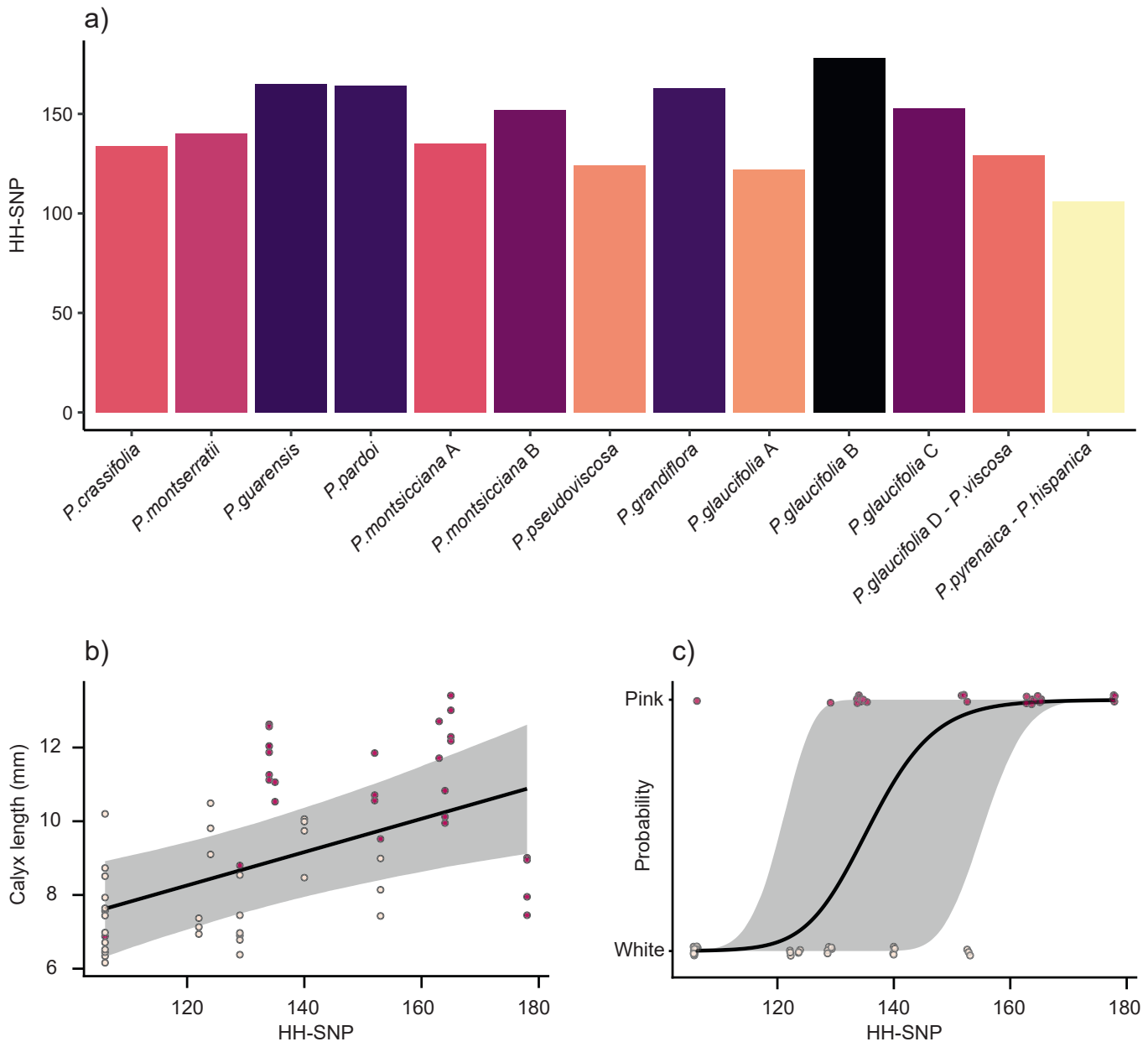

Fig. 7. a) Number of highly heterozygous SNPs per genetic group. Bars indicate the number of loci exceeding the Ho frequency threshold (≥0.75), revealing marked differences in genomic heterozygosity among lineages. b-c) Posterior predictions from the Gaussian phylogenetic mixed model for calyx length and binomial phylogenetic mixed model for petal colour. The solid line represents the posterior mean, and the shaded region indicates the 95% highest posterior density (HPD) interval. Coloured points depict populations with white and pink corollas.

Despite this complexity, our HybSeq-based approach resolves many longstanding systematic uncertainties within *Petrocoptis*. Using hundreds of nuclear low-copy loci and complete plastome data, we recovered most morphologically circumscribed species (Montserrat & Fernández-Casas, 1990) as monophyletic and obtained robust support for several major lineages.

The *Petrocoptis pyrenaica–P. hispanica* complex is resolved as sister to the rest of the genus, followed by a deep split into two geographically structured clades corresponding broadly to the Cantabrian and the Pyrenean–Iberian mountain systems. This geographic signal supports the view that the genus diversified largely *in situ* within the northern Iberian limestone mountain systems, where orographic complexity and Quaternary climatic oscillations likely promoted repeated cycles of population isolation, persistence in local refugia, and secondary contact. Comparable phylogeographic and evolutionary patterns have been reported for several montane plant lineages from the Pyrenees and the Cantabrian Range, highlighting the role of northern Iberian mountain systems as centres of Quaternary diversification (Peredo et al., 2009; Charrier et al., 2014; Liberal et al., 2014; Schuler et al., 2022; Carnicero et al., 2022; Pomeda-Gutiérrez et al., 2023; Garnatje et al., 2023).

Within the Cantabrian lineage, our phylogenomic analyses reveal a complex internal structure composed of several well-supported nuclear lineages combined with pronounced cytonuclear discordance. Plastid relationships are frequently incongruent with nuclear affinities, and different lineages traditionally included within *Petrocoptis glaucifolia* are resolved in multiple, distantly related positions, resulting in a clearly polyphyletic pattern. This discordance can at least partly be explained by repeated episodes of introgression and organellar capture that were not accompanied by phenotypic differentiation. Overall, the Cantabrian clade exemplifies how reticulate processes can generate intricate genomic architectures that depart from strictly bifurcating evolutionary histories.

The central Pyrenean-Iberian and eastern Pyrenean range clade exhibits an even stronger signal of reticulate evolution. Network analyses consistently recover multiple reticulation events (Fig. 3), with the clearest case involving the species *Petrocoptis pardoi*, which shows mixed nuclear ancestry derived from lineages related to current *P. montsicciana–P. pseudoviscosa* and *P. guarensis-P. montserratii*. Given that all species of *Petrocoptis* are diploid and there is no evidence for polyploidization in the genus, this pattern is best interpreted as ancestral homoploid hybridization rather than genome duplication. The genomic admixture detected in *P. pardoi*, together with its intermediate morphological features, supports a hybrid origin resulting from historical gene flow between divergent lineages. More broadly, the prevalence of reticulation within this clade highlights ancient hybridization as a major driver of genomic complexity in *Petrocoptis*, substantially shaping species relationships even at relatively shallow phylogenetic scales.

4.2. Evolutionary and functional significance of seed traits in Petrocoptis: an adaptive syndrome related to water uptake on vertical cliffs

Our comparative analyses of reproductive traits clarify how genetic history, geography and selection interact to shape phenotypic evolution in *Petrocoptis*. Seed morphology has long been considered taxonomically informative in the genus. Here we show that it exhibits a general phylogenetic structure but also repeated shifts in adaptive optima.

Contrary to classical eco-evolutionary expectations linking large seeds to benign, low-stress environments and small seeds to harsher conditions (Chen et al., 2022; Moles and Westoby, 2004), our phylogenetically controlled analyses detect no significant association between seed size and climatic variables (Table S9). This result suggests that seed size alone is unlikely to represent the primary target of selection across environmental gradients in *Petrocoptis*. Instead, climatic associations are concentrated in strophiolar traits (Fig. S6). Larger strophioles and higher strophiole-to-seed ratios are consistently correlated with hotter and drier conditions, pointing to a functional role of the strophiole.

These patterns support the hypothesis that strophiolar hairs act as water-regulating structures during germination, enhancing seeds performance under episodic water availability in xeric microhabitats such as vertical cliffs. This interpretation is reinforced by recent experimental evidence showing that the mucilaginous hairs of *Petrocoptis* strophioles can significantly improve water uptake under dry conditions (Calvo-Yuste et al., 2024). In cliff-dwelling species, where soil is scarce and moisture pulses are brief and unpredictable, selection is therefore likely to act more strongly on traits that mediate effective hydration at the seed–substrate interface than on seed size itself.

Ornstein–Uhlenbeck modelling further indicates that seed size, strophiole relative size, and strophiolar hair morphology have evolved in a coordinated manner, defining distinct adaptive regimes (Fig. 4). Lineages bearing cylindrical hairs tend to produce small seeds coupled with proportionally large strophioles, whereas lineages with claviform hairs are characterized by larger seeds and relatively reduced strophioles. These contrasting syndromes suggest alternative adaptive strategies to overcome water limitation during germination. One strategy involves investing in numerous fine hairs to maximize surface area and water absorption, whereas the other relies on fewer but thicker hairs with greater individual water-holding capacity. Mixed phenotypes may represent transitional evolutionary states or reflect relaxed or heterogeneous selection on this trait complex.

Taken together, these results support the existence of a seed–strophiole adaptive syndrome in *Petrocoptis*, shaped primarily by microclimatic water availability rather than by seed size per se. They further emphasize that subtle modifications of accessory seed structures can have major ecological significance in extreme habitats, such as limestone cliffs, where successful germination depends on efficiently exploiting limited water inputs. To fully validate this functional interpretation, future work should move beyond comparative inference and directly test the ecological performance of seeds. Controlled experiments are needed to quantify the capacity of the strophioles from different lineages and climatically contrasting populations to capture and retain water or atmospheric moisture under xeric conditions. It will also be essential to determine how variation in strophiole morphology translates into differences in germination success and early seedling establishment. Such empirical tests will be essential to confirm the adaptive value of the seed–strophiole syndromes inferred here and to link morphological diversification more explicitly to fitness in natural environments.

Beyond *Petrocoptis*, a broader comparative perspective suggests that strophioles may represent a recurrent, yet still poorly understood, solution to the challenges imposed by rocky habitats. By cross-referencing a curated list of Iberian rupicolous taxa, restricted to frequent, preferential and strict cliff-dwelling taxa (Cliff Affinity Index $>$ 2.5; Lorite et al., 2026), with published inventories of species bearing a strophiole (Ortega-Olivencia et al 2021), we found that nearly one fifth of Iberian species with a strophiole are associated with rocky habitats. This pattern hints at a possible ecological filtering effect, whereby strophiolar structures may be selectively favoured in environments characterized by shallow substrates, rapid drainage and intermittent water availability. This observation also underscores a broader gap in functional trait research. Despite their repeated evolution and putative adaptive significance, strophioles, arils and related appendages remain largely absent from functional trait frameworks. Integrating detailed morphological, anatomical and experimental data on these structures across independent rupicolous lineages will be essential to assess whether the seed–strophiole syndrome documented in *Petrocoptis* reflects a broader, convergent response to water limitation during germination in extreme rocky habitats, or a lineage-specific innovation amplified by historical contingency.

4.3. Coevolution of floral traits in Petrocoptis

Floral traits in *Petrocoptis* exhibit clear adaptive patterns but are only partially aligned with the deep phylogenetic structure of the genus. Floral characters are widely recognized as evolutionarily labile and prone to rapid divergence in response to changes in pollination environment and mating systems (Fenster et al., 2004; Smith, 2010). As a result, floral traits may evolve at microevolutionary scales that are decoupled from major clade divergence, leading to repeated and independent trait shifts across lineages (Smith, 2010). Empirical studies in diverse angiosperm groups have documented similar patterns of convergent and homoplastic evolution in floral colour and size, often driven by pollinator-mediated selection (Schiestl and Johnson, 2013; Gervasi and Schiestl, 2017).

Consistent with these expectations, our ancestral character reconstructions and Ornstein-Uhlenbeck models indicate that calyx length has increased repeatedly across the evolution of *Petrocoptis* and that these shifts are tightly associated with changes in flower colour. Pink-flowered lineages consistently exhibit longer calyces than white-flowered ones. However, these trait combinations arise independently in different parts of the phylogeny rather than being confined to a single lineage. This coordinated evolution of colour and size suggests pollinator-mediated selection: in many angiosperms, floral size and hue covary because different pollinators respond to distinct visual and morphological cues (Van der Niet et al., 2014; Trunschke et al., 2017). The repeated association of pink flowers with larger floral structures in *Petrocoptis* is therefore best interpreted as the outcome of recurrent adaptive responses to similar pollination-mediated selective pressures, rather than as a legacy of shared ancestry (Van der Niet et al., 2014).

This pattern parallels empirical findings in closely related taxa within the tribe Sileneae: empirical studies in *Silene* sect. *Physolychnis* have found that suites of floral traits do not always cluster by phylogenetic affinity but can instead reflect convergent responses to similar selective pressures, even when species share a recent common ancestry, suggesting that ecological factors and ancestral variation may shape

floral diversity as much as lineage divergence (Berardi et al., 2022). Our results indicate that *Petrocoptis* conforms to this broader evolutionary framework: floral traits are evolutionarily labile and can diverge rapidly within and across lineages, obscuring any simple correspondence between floral phenotype and phylogenetic position.

Patterns of character evolution inferred from our phylogenetic reconstructions further reinforce this view. The equal-rates model best explains petal colour evolution, implying similar probabilities of transitions between white and pink. Stochastic character mapping reveals multiple independent gains of pink corollas across all major clades, as well as several reversals to white, a dynamic that closely mirrors repeated shifts in calyx length optima. Such recurrent, coordinated changes are unlikely to result from neutral drift and instead point to repeated episodes of adaptive divergence in pollination ecology.

Importantly, small, white flowers are consistently reconstructed as ancestral, whereas large, pink flowers are derived, in agreement with the reproductive biology of extant species. For example, *Petrocoptis viscosa* bears small white flowers associated with high levels of autogamy and a narrow visitor spectrum, whereas *P. grandiflora* produces large pink flowers dependent on long-tongued bees and shows reduced reproductive success under selfing (Navarro et al., 1993; Navarro and Guitián, 2002). These contrasts exemplify how floral traits can shift repeatedly and independently in response to pollinator-mediated selection, rather than tracking phylogenetic splits.

4.4. Floral phenotypes are associated with genetic diversity in Petrocoptis

As strict chasmophytes, *Petrocoptis* species display a suite of reproductive traits that enhance local recruitment on vertical limestone walls. Flower stems are characteristically reoriented toward the rock surface once the fruit has ripened, favouring seed release directly into adjacent crevices (i.e., geoautochory, active geocarpy according to Barker, 2005; Llorens, 1982; Ellison and Gotelli, 2001). In addition, hygroscopic strophiolar hairs facilitate adhesion to the substrate, and, as shown here, likely play a key role in water capture under xeric and episodic moisture regimes. However, restricted dispersal combined with patchily distributed cliff environments is expected to increase spatial genetic structuring and may generate demographic conditions conducive to reduced effective population size and a decrease of genetic diversity over evolutionary time.

Our ancestral reconstructions further indicate that early-diverging *Petrocoptis* lineages likely bore small, white, self-compatible flowers. The evolution of self-compatibility is well known to promote reproductive assurance under mate or pollinator limitation, but it is also consistently associated with increased homozygosity and reduced within-population genetic diversity (Hamrick and Godt, 1996; Charlesworth and Charlesworth, 1999; Glémin and Ronfort, 2013). Although low genetic diversity and high selfing rates are not necessarily incompatible with ecological persistence (indeed, many selfing lineages remain demographically stable for extended periods; Barrett, 2002; Wright et al., 2013a; Wright et al., 2013b), reduced standing genetic variation may constrain long-term adaptive potential, particularly under changing environmental conditions. In this context, shifts toward increased floral conspicuousness and traits promoting outcrossing may represent evolutionary pathways restoring genomic heterozygosity and enhancing adaptive flexibility.

Under this ecological–genetic framework, the recurrent evolution of more conspicuous floral phenotypes, with larger calyces and pink corollas, can be interpreted as a y mechanism enhancing pollinator-mediated connectivity among otherwise isolated populations. In other words, while seed traits promote local persistence through autochorous establishment, floral elaboration may increase opportunities for outcrossing across spatially segregated cliff populations, counterbalancing the potential genetic consequences of restricted dispersal.

Our phylogenetically informed analyses further demonstrate that this microevolutionary lability of floral traits is closely linked to genomic diversity. Both calyx length and corolla colour are strongly correlated with HH-SNP, our proxy to genomic heterozygosity. Lineages with higher genomic diversity tend to develop larger flowers and are more likely to exhibit pink corollas, whereas lineages with reduced heterozygosity predominantly retained small, white flowers.

This pattern suggests that floral phenotype and genetic diversity evolve jointly, potentially reflecting variation in effective population size, mating system or historical gene flow. Larger, pigmented flowers may promote outcrossing and pollinator-mediated selection, processes expected to maintain or increase heterozygosity. Conversely, small white flowers are commonly associated with self-compatible systems, which can reduce effective recombination and genomic diversity through prolonged selfing or demographic bottlenecks. Under this framework, higher heterozygosity may facilitate the maintenance of standing genetic variation underlying floral traits, thereby enhancing the capacity for adaptive responses during diversification.

These results align with theoretical and empirical work demonstrating strong feedbacks between mating system evolution, genetic diversity and adaptive potential (Charlesworth and Wright, 2001; Novikova et al., 2022; Slotte et al., 2013; Wright et al., 2013a; Wright et al., 2013b). The predominance of white, self-compatible flowers near the root of the *Petrocoptis* phylogeny supports a scenario in which selfing would be the primitive mating system in the genus. However, the repeated, independent emergence of presumably more outcrossing lineages showing larger calyces and pink flowers, indicates that floral evolution in *Petrocoptis* is not strictly constrained by deep phylogenetic history. Although transitions from selfing to outcrossing are generally considered rare and asymmetric (Igic and Busch, 2013; Takebayashi and Morrell, 2001), recent work suggests that ecological context and demographic processes can facilitate such reversals (García-Muñoz et al., 2025). In *Petrocoptis*, pollinator-mediated selection acting on genetically diverse populations may have repeatedly enabled microevolutionary shifts in floral traits that transcend the boundaries of major clades.

5. Conclusion

By integrating phylogenomics, species tree inference and detailed morphological analyses, this study provides the most comprehensive evolutionary framework for the Iberian endemic genus *Petrocoptis* to date, revealing diversification across multiple evolutionary scales. Our phylogenomic analyses establish a robust historical scaffold, showing that the tangled phylogeny of the genus results from rapid lineage splitting combined with reticulate evolution, including ancient hybridization and ILS, which together generate a mosaic genomic architecture and widespread cytonuclear discordance. Within this reticulate genomic context, reproductive traits emerge as dynamic and partially decoupled components of diversification. Our results provide an evidence of an adaptive syndrome associated to strophiolar structures which enhance germination under the moisture limiting conditions of limestone cliffs and show that floral traits are evolutionarily labile and frequently independent of major phylogenetic divisions. Instead, floral diversification reflects recurrent, convergent microevolutionary responses associated to genomic diversity. Lineages with higher genomic heterozygosity tend to exhibit larger calyces and pink corollas, suggesting that standing genetic variation facilitates rapid adaptive responses, while lineages with reduced diversity retain small, white, self-compatible flowers. Although the associations documented here are robust and phylogenetically informed, they remain correlative. Establishing causality will require integrative approaches combining population genomics, explicit quantification of pollen flow and selfing rates, detailed characterization of pollinator assemblages, and experimental analyses of seed germination under controlled moisture regimes, alongside with efforts to elucidate the genetic architecture underlying floral and seed traits. Although our sampling encompasses the broad geographic and morphological diversity currently recognized within *Petrocoptis*, increased population-level sampling in some narrowly distributed taxa

may further refine species boundaries and patterns of monophyly. Taken together, these results underscore how reticulate evolution, ecological selection and microevolutionary adaptation jointly shape genomic complexity and phenotypic diversity in *Petrocoptis*, illustrating that even small, insular-like distributed chasmophytic genera can harbor mosaic genomes and rapidly evolving traits. Such complexity is likely widespread in geographically fragmented, stress-prone landscapes, where reticulate evolution and rapid adaptation often operate in concert to generate botanical diversity.

CRediT authorship contribution statement

Jorge Calvo-Yuste: Writing – review & editing, Writing – original draft, Visualization, Validation, Software, Methodology, Investigation, Formal analysis, Data curation, Conceptualization. **M.Montserrat Martínez-Ortega:** Writing – review & editing, Supervision, Resources, Project administration, Methodology, Investigation, Funding acquisition, Conceptualization. **Teresa Malvar Ferreras:** Writing – review & editing, Methodology. **Juan Viruel:** Writing – review & editing, Methodology, Investigation, Conceptualization. **Pablo Tejero:** Writing – review & editing, Supervision, Resources, Project administration, Methodology, Investigation, Funding acquisition, Conceptualization.

Funding

This research was supported by the project PRIOCONEX, funded by FUNDACIÓN BIODIVERSIDAD (MINISTERIO PARA LA TRANSICIÓN ECOLÓGICA Y EL RETO DEMOGRÁFICO, SPANISH GOVERNMENT, Resolución 10/11/2020), by the MINISTERIO DE CIENCIA, INNOVACIÓN Y UNIVERSIDADES through a PhD scholarship (FPU21/00305 to J.C.-Y.), by the Predoctoral Contract Program III of the Universidad de Salamanca, funded in collaboration with Banco Santander (2021 call, to J.C.-Y.), and by RYC2023-042611-I by MCIU/AEI/10.13039/501100011033 and FSE+ to J.V.

Data Statement

The sequences for this study have been deposited in the European Nucleotide Archive (ENA) at EMBL-EBI under accession number PRJEB112852. Other data generated in this study, including processed datasets, and R scripts used for phylogenetic and comparative analyses, are publicly available in Zenodo at https://doi.org/10.5281/zenodo.18816034.

Declaration of competing interest

The authors declare that they have no known competing financial interests or personal relationships that could have appeared to influence the work reported in this paper.

Acknowledgments

We sincerely thank all collaborators who contributed to this project, particularly those involved in the extensive field sampling efforts. We are especially grateful to Parque Nacional de Ordesa y Monte Perdido and Parque Nacional de los Picos de Europa for logistical support, as well as to the biodiversity and environmental authorities of Galicia, Asturias, Castilla y León, Cantabria, Euskadi (Araba and Gipuzkoa), Navarra, Aragón, Catalunya and Comunitat Valenciana for their collaboration and for granting collecting permits.

We thank the curators and staff of the following herbaria for providing material for this study: JACA, SALA, MA, VIT, VAL, LEB, BIO and SANT (listed in order of contribution).

Scanning Electron Microscopic images were captured at the University of Oviedo thanks to the invaluable help of our colleagues B. Adolfo Vallina-Rodríguez, Borja Jiménez-Alfaro, Clara Espinosa del Alba and Víctor González-García.

Computational analyses were performed using the high-performance computing facilities of Supercomputación de Castilla y León (SCAYLE; https://www.scayle.es/), whose support is gratefully acknowledged.

We are particularly indebted to Luis Navarro for valuable discussions and for generously sharing unpublished data that contributed to this work. We also thank Dr. Lihua Yang (South China Botanical Garden) for helpful comments on the implementation of the DendroPy pipeline.

Appendix A. Supplementary data

Supplementary data to this article can be found online at https://doi.org/10.1016/j.ympev.2026.108648.

Data availability

Research Link Provided in the “Data Statement” section

References

Allman, E.S., Baños, H., Rhodes, J.A., 2019. NANUQ: A method for inferring species networks from gene trees under the coalescent model. Algorithms Mol. Biol. 14, 1–25. https://doi.org/10.1186/S13015-019-0159-2/FIGURES/14.

Allman, E.S., Mitchell, J.D., Rhodes, J.A., 2022. Gene Tree Discord, Simplex Plots, and Statistical Tests under the Coalescent. Syst. Biol. 71, 929–942. https://doi.org/10.1093/SYSBIO/SYAB008.

Anderson, E., Stebbins, G.L., 1954. Hybridization as an Evolutionary Stimulus. Evolution (N Y). 8, 378. https://doi.org/10.2307/2405784.

Andrews, S., 2014. FastQC A Quality Control tool for High Throughput Sequence Data [WWW Document]. URL https://www.bioinformatics.babraham.ac.uk/projects/fastqc/ (accessed 7.4.25).

Antonelli, A., Kissling, W.D., Flantua, S.G.A., Bermúdez, M.A., Mulch, A., Muellner-Riehl, A.N., Kreft, H., Linder, H.P., Badgley, C., Fjeldså, J., Fritz, S.A., Rahbek, C., Herman, F., Hooghiemstra, H., Hoorn, C., 2018. Geological and climatic influences on mountain biodiversity. Nature Geoscience 2018 11:10 11, 718–725. Doi: 10.1038/s41561-018-0236-z.

Armbruster, W.S., 2014. Floral specialization and angiosperm diversity: phenotypic divergence, fitness trade-offs and realized pollination accuracy. AoB Plants 6. https://doi.org/10.1093/AOBPLA/PLU003.

Avise, J.C., 2000. Phylogeography. Harvard University Press. Doi: 10.2307/j.ctv1nzfgj7.

Badgley, C., Smiley, T.M., Terry, R., Davis, E.B., DeSantis, L.R.G., Fox, D.L., Hopkins, S.S.B., Jezkova, T., Matocq, M.D., Matzke, N., McGuire, J.L., Mulch, A., Riddle, B.R., Roth, V.L., Samuels, J.X., Strömberg, C.A.E., Yanites, B.J., 2017. Biodiversity and Topographic Complexity: Modern and Geohistorical Perspectives. Trends Ecol. Evol. 32, 211–226. https://doi.org/10.1016/J.TREE.2016.12.010.

Bankevich, A., Nurk, S., Antipov, D., Gurevich, A.A., Dvorkin, M., Kulikov, A.S., Lesin, V.M., Nikolenko, S.I., Pham, S., Prjibelski, A.D., Pyshkin, A.V., Sirotkin, A.V., Vyahhi, N., Tesler, G., Alekseyev, M.A., Pevzner, P.A., 2012. SPAdes: a new genome assembly algorithm and its applications to single-cell sequencing. J. Comput. Biol. 19, 455–477. https://doi.org/10.1089/CMB.2012.0021.

Barker, N.P., 2005. A review and survey of basicarpy, geocarpy and amphicarpy in the African and Madagascan flora. Ann. Mo. Bot. Gard. 92, 445–462.

Barrett, S.C.H., 2002. The evolution of plant sexual diversity. Nature Reviews Genetics 2002 3:4 3, 274–284. Doi: 10.1038/nrg776.

Baskin, C.C., Baskin, J.M., 2014. Seeds : ecology, biogeography, and evolution of dormancy and germination. Elsevier Science.

Berardi, A.E., Betancourt Morejón, A.C., Hopkins, R., 2022. Convergence without divergence in North American red-flowering Silene. Front. Plant Sci. 13, 945806. https://doi.org/10.3389/FPLS.2022.945806/BIBTEX.

Blair, C., Ané, C., 2020. Phylogenetic trees and networks can serve as powerful and complementary approaches for analysis of genomic data. Syst. Biol. 69, 593–601. https://doi.org/10.1093/SYSBIO/SYZ056.

Blomberg, S.P., Garland, T., Ives, A.R., 2003. Testing for phylogenetic signal in comparative data: behavioral traits are more labile. Evolution 57, 717–745. https://doi.org/10.1111/J.0014-3820.2003.TB00285.X.

Bolger, A.M., Lohse, M., Usadel, B., 2014. Trimmomatic: a flexible trimmer for Illumina sequence data. Bioinformatics 30, 2114–2120. https://doi.org/10.1093/BIOINFORMATICS/BTU170.

Borowiec, M.L., 2016. AMAS: A fast tool for alignment manipulation and computing of summary statistics. PeerJ 2016, e1660.

Cai, L., Xi, Z., Lemmon, E.M., Lemmon, A.R., Mast, A., Buddenhagen, C.E., Liu, L., Davis, C.C., 2021. The perfect storm: gene tree estimation error, incomplete lineage sorting, and ancient gene flow explain the most recalcitrant ancient angiosperm clade. Malpighiales. Syst. Biol. 70, 491–507. https://doi.org/10.1093/SYSBIO/SYAA083.

Calvo-Yuste, J., Ruiz-Rodríguez, Á.L., Hermosilla, B., Agut, A., Martínez-Ortega, M.M., Tejero, P., 2024. Classification importance of seed morphology and insights on large-scale climate-driven strophiole size changes in the iberian endemic chasmophytic genus *Petrocoptis* (Caryophyllaceae). Plants 13, 3208. https://doi.org/10.3390/PLANTS13223208/S1.

Capella-Gutiérrez, S., Silla-Martínez, J.M., Gabaldón, T., 2009. trimAl: a tool for automated alignment trimming in large-scale phylogenetic analyses. Bioinformatics 25, 1972–1973. https://doi.org/10.1093/BIOINFORMATICS/BTP348.
Carnicero, P., Wessely, J., Moser, D., Font, X., Dullinger, S., Schönswetter, P., 2022. Postglacial range expansion of high-elevation plants is restricted by dispersal ability and habitat specialization. J. Biogeogr. 49, 1739–1752. https://doi.org/10.1111/JBI.14390.
Charlesworth, B., Charlesworth, D., 1999. The genetic basis of inbreeding depression. Genet. Res. (Camb) 74, 329–340. https://doi.org/10.1017/S0016672399004152.
Charlesworth, D., Wright, S.I., 2001. Breeding systems and genome evolution. Curr. Opin. Genet. Dev. 11, 685–690. https://doi.org/10.1016/S0959-437X(00)00254-9.
Charrier, O., Dupont, P., Pornon, A., Escaravage, N., 2014. Microsatellite marker analysis reveals the complex phylogeographic history of *Rhododendron ferrugineum* (Ericaceae) in the Pyrenees. PLoS One 9. https://doi.org/10.1371/JOURNAL.PONE.0092976.
Chen, K., Burgess, K.S., He, F., Yang, X.Y., Gao, L.M., Li, D.Z., 2022. Seed traits and phylogeny explain plants' geographic distribution. Biogeosciences 19, 4801–4810. https://doi.org/10.5194/BG-19-4801-2022.
Chernomor, O., Von Haeseler, A., Minh, B.Q., 2016. Terrace Aware Data Structure for Phylogenomic Inference from Supermatrices. Syst. Biol. 65, 997–1008. https://doi.org/10.1093/SYSBIO/SYW037.
Chifman, J., Kubatko, L., 2014. Quartet Inference from SNP Data Under the Coalescent Model. Bioinformatics 30, 3317–3324. https://doi.org/10.1093/BIOINFORMATICS/BTU530.
Cires, E., Prieto, J.A.F., 2015. Phylogenetic relationships of *Petrocoptis* A. Braun ex Endl. (Caryophyllaceae), a discussed genus from the Iberian Peninsula. J. Plant Res. 128, 223–238. https://doi.org/10.1007/S10265-014-0691-6/TABLES/4.
Clavel, J., Escarguel, G., Merceron, G., 2015. mvmorph: an r package for fitting multivariate evolutionary models to morphometric data. Methods Ecol. Evol. 6, 1311–1319. https://doi.org/10.1111/2041-210X.12420.
Coyne, J.A., Orr, H.A., 2004. Speciation. Sinauer Associates, Sunderland.
Csiba, L., Powell, M.P., 2006. Isolation of total plant celular DNA for long-term storage: CTAB procedure. , in: Savolainen, V., Powell, M.P., Davis, K., Reeves, G., Corthals, A. (Eds.), DNA and Tissue Banking for Biodiversity and Conservation: Theory, Practice and Uses. Richmond, pp. 114–117.
Degnan, J.H., Rosenberg, N.A., 2009. Gene tree discordance, phylogenetic inference and the multispecies coalescent. Trends Ecol. Evol. 24, 332–340. https://doi.org/10.1016/J.TREE.2009.01.009/ATTACHMENT/D17EC0EE-1965-49B4-BF5E-6EE9FBF86503/MMC1.PDF.
Depristo, M.A., Banks, E., Poplin, R., Garimella, K. V., Maguire, J.R., Hartl, C., Philippakis, A.A., Del Angel, G., Rivas, M.A., Hanna, M., McKenna, A., Fennell, T.J., Kernytsky, A.M., Sivachenko, A.Y., Cibulskis, K., Gabriel, S.B., Altshuler, D., Daly, M. J., 2011. A framework for variation discovery and genotyping using next-generation DNA sequencing data. Nature Genetics 2011 43:5 43, 491–498. Doi: 10.1038/ng.806.
Dilley, J.D., Wilson, P., Mesler Dilley, M.R., Wilson, J.D., Mesler, P., Dilley, J.D., Wilson, P., Mesler, M.R., 2000. The radiation of *Calochortus*: generalist flowers moving through a mosaic of potential pollinators. Oikos 89, 209–222. https://doi.org/10.1034/J.1600-0706.2000.890201.X.
Edwards, S.V., Xi, Z., Janke, A., Faircloth, B.C., McCormack, J.E., Glenn, T.C., Zhong, B., Wu, S., Lemmon, E.M., Lemmon, A.R., Leaché, A.D., Liu, L., Davis, C.C., 2016. Implementing and testing the multispecies coalescent model: a valuable paradigm for phylogenomics. Mol. Phylogenet. Evol. 94, 447–462. https://doi.org/10.1016/J.YMPEV.2015.10.027.
Ellison, A.M., Gotelli, N.J., 2001. Evolutionary ecology of carnivorous plants. Trends Ecol. Evol. 16, 623–629. https://doi.org/10.1016/S0169-5347(01)02269-8/ASSET/D9AFB806-B3D3-4397-9E4F-AFA145231B5C/MAIN.ASSETS/GRBOX2.JPG.
ESRI, 2020. ArcGIS Desktop: Release 10.8.1.
Ewels, P., Magnusson, M., Lundin, S., Käller, M., 2016. MultiQC: summarize analysis results for multiple tools and samples in a single report. Bioinformatics 32, 3047–3048. https://doi.org/10.1093/BIOINFORMATICS/BTW354.
Fehrer, J., Gemeinholzer, B., Chrtek, J., Bräutigam, S., 2007. Incongruent plastid and nuclear DNA phylogenies reveal ancient intergeneric hybridization in *Pilosella* hawkweeds (Hieracium, Cichorieae, Asteraceae). Mol. Phylogenet. Evol. 42, 347–361. https://doi.org/10.1016/J.YMPEV.2006.07.004.
Felsenstein, J., 1985. Phylogenies and the comparative method. Am. Nat. 125, 1–15. https://doi.org/10.1086/284325.
Fenster, C.B., Armbruster, W.S., Wilson, P., Dudash, M.R., Thomson, J.D., 2004. Pollination Syndromes and Floral Specialization. Annu. Rev. Ecol. Evol. Syst. 35, 375–403. https://doi.org/10.1146/annurev.ecolsys.34.011802.132347.
Folk, R.A., Mandel, J.R., Reudenstein, J.V.F., 2017. Ancestral Gene Flow and Parallel Organellar Genome Capture Result in Extreme Phylogenomic Discord in a Lineage of Angiosperms. Syst. Biol. 66, 320–337. https://doi.org/10.1093/SYSBIO/SYW083.
García, N., Folk, R.A., Meerow, A.W., Chamala, S., Gitzendanner, M.A., de Oliveira, R.S., Soltis, D.E., Soltis, P.S., 2017. Deep reticulation and incomplete lineage sorting obscure the diploid phylogeny of rain-lilies and allies (Amaryllidaceae tribe Hippeastreae). Mol. Phylogenet. Evol. 111, 231–247. https://doi.org/10.1016/J.YMPEV.2017.04.003.
García-Muñoz, A., Ferrón, C., Vaca-Benito, C., Olmedo-Castellanos, C., Martínez-Gómez, M.N., López-Pérez, T., Bakkali, M., Castro, S., Castro, M., Loureiro, J., Muñoz-Pajares, A.J., Abdelaziz, M., 2025. Can ploidy changes propel the evolution of allogamy in a selfing species complex? BMC Plant Biol. 25, 1–15. https://doi.org/10.1186/S12870-025-06868-1/TABLES/3.
Garnatje, T., Catalán, P., Inda, L.A., Vallès, J., Pyke, S., 2023. Genome size of grass *Festuca* mountain species from the southwestern European Pyrenees: variation, evolution, and new assessments. Plant Syst. Evol. 309, 29-. https://doi.org/10.1007/S00606-023-01867-X/TABLES/1.
Gervasi, D.D.L., Schiestl, F.P., 2017. Real-time divergent evolution in plants driven by pollinators. Nature Communications 2017 8:1 8, 1–8. Doi: 10.1038/ncomms14691.
Glémin, S., Ronfort, J., 2013. Adaptation and maladaptation in selfing and outcrossing species: New mutations versus standing variation. Evolution (N Y). 67, 225–240. https://doi.org/10.1111/J.1558-5646.2012.01778.X.
Green, P.J., 1995. Reversible jump Markov chain Monte Carlo computation and Bayesian model determination. Biometrika 82, 711–732. https://doi.org/10.1093/BIOMET/82.4.711.
Guindon, S., Dufayard, J.F., Lefort, V., Anisimova, M., Hordijk, W., Gascuel, O., 2010. New algorithms and methods to estimate maximum-likelihood phylogenies: assessing the performance of PhyML 3.0. Syst. Biol. 59, 307–321. https://doi.org/10.1093/SYSBIO/SYQ010.
Gutterman, Y., 2000. Maternal effects on seeds during development., in: Seeds: The Ecology of Regeneration in Plant Communities. CABI Publishing, UK, pp. 59–84. Doi: 10.1079/9780851994321.0059.
Hadfield, J.D., 2010. MCMC methods for multi-response generalized linear mixed models: the MCMCglmm R package. J. Stat. Softw. 33, 1–22. https://doi.org/10.18637/JSS.V033.I02.
Hamrick, J.L., Godt, M.J.W., 1996. Effects of life history traits on genetic diversity in plant species. Philos. Trans. R. Soc., B 351, 1291–1298. https://doi.org/10.1098/RSTB.1996.0112.
Harper, J.L., Lovell, P.H., Moore, K.G., 1970. The Shapes and Sizes of Seeds. Annu. Rev. Ecol. Syst. 1, 327–356. https://doi.org/10.1146/annurev.es.01.110170.001551.
Heidelberger, P., Welch, P.D., 1981. A spectral method for confidence interval generation and run length control in simulations. Commun. ACM 24, 233–245. https://doi.org/10.1145/358598.358630/ASSET/09EF8325-4E32-478A-97C4-A7A61EC8620E/ASSETS/358598.358630.FP.PNG.
Hewitt, G., 2000. The genetic legacy of the Quaternary ice ages. Nature 2000 405:6789 405, 907–913. Doi: 10.1038/35016000.
Holmgren, P.K., Holmgren, N.H., Barnett, L.C., 1990. Index herbariorum. Part I: the herbaria of the world. Regnum vegetabile. New York Botanical Gardens 120.
Huelsenbeck, J.P., Nielsen, R., Bollback, J.P., 2003. Stochastic mapping of morphological characters. Syst. Biol. 52, 131–158. https://doi.org/10.1080/10635150390192780.
Hughes, C., Eastwood, R., 2006. Island radiation on a continental scale: exceptional rates of plant diversification after uplift of the Andes. PNAS 103, 10334–10339. https://doi.org/10.1073/PNAS.0601928103.
Hughes, C.E., Pennington, R.T., Antonelli, A., 2013. Neotropical plant evolution: assembling the big picture. Bot. J. Linn. Soc. 171, 1–18. https://doi.org/10.1111/BOJ.12006.
Huson, D.H., Bryant, D., 2024. The SplitsTree App: interactive analysis and visualization using phylogenetic trees and networks. Nature Methods 2024 21:10 21, 1773–1774. Doi: 10.1038/s41592-024-02406-3.
Igic, B., Busch, J.W., 2013. Is self-fertilization an evolutionary dead end? New Phytol. 198, 386–397. https://doi.org/10.1111/NPH.12182.
Johnson, M.G., Gardner, E.M., Liu, Y., Medina, R., Goffinet, B., Shaw, A.J., Zerega, N.J. C., Wickett, N.J., 2016. HybPiper: extracting coding sequence and introns for phylogenetics from high-throughput sequencing reads using target enrichment. Appl. Plant Sci. 4, apps.1600016. https://doi.org/10.3732/APPS.1600016.
Johnson, M.G., Pokorny, L., Dodsworth, S., Botigué, L.R., Cowan, R.S., Devault, A., Eiserhardt, W.L., Epitawalage, N., Forest, F., Kim, J.T., Leebens-Mack, J.H., Leitch, I. J., Maurin, O., Soltis, D.E., Soltis, P.S., Wong, G.K.S., Baker, W.J., Wickett, N.J., 2019. A universal probe set for targeted sequencing of 353 nuclear genes from any flowering plant designed using k-medoids clustering. Syst. Biol. 68, 594–606. https://doi.org/10.1093/SYSBIO/SYY086.
Kalyaanamoorthy, S., Minh, B.Q., Wong, T.K.F., Von Haeseler, A., Jermiin, L.S., 2017. ModelFinder: fast model selection for accurate phylogenetic estimates. Nature Methods 2017 14:6 14, 587–589. Doi: 10.1038/nmeth.4285.
Katoh, K., Standley, D.M., 2013. MAFFT Multiple Sequence Alignment Software Version 7: Improvements in Performance and Usability. Molecular Biology and Evolution 30 (4), 772–780. https://doi.org/10.1093/molbev/mst010.
Kay, K.M., Sargent, R.D., 2009. The role of animal pollination in plant speciation: integrating ecology, geography, and genetics. Annu. Rev. Ecol. Evol. Syst. 40, 637–656. https://doi.org/10.1146/annurev.ecolsys.110308.120310.
Kück, P., Longo, G.C., 2014. FASconCAT-G: extensive functions for multiple sequence alignment preparations concerning phylogenetic studies. Front. Zool. 11, 1–8. https://doi.org/10.1186/S12983-014-0081-X/FIGURES/2.
Larson, D.W., Matthes, U., Kelly, P.E., 2000. Cliff Ecology: pattern and process in cliff ecosystems. Cambridge University Press. Doi: 10.1017/CBO9780511525582.
Leebens-Mack, J.H., Barker, M.S., Carpenter, E.J., Deyholos, M.K., Gitzendanner, M.A., Graham, S.W., Grosse, I., Li, Z., Melkonian, M., Mirarab, S., Porsch, M., Quint, M., Rensing, S.A., Soltis, D.E., Soltis, P.S., Stevenson, D.W., Ullrich, K.K., Wickett, N.J., DeGironimo, L., Edger, P.P., Jordon-Thaden, I.E., Joya, S., Liu, T., Melkonian, B., Miles, N.W., Pokorny, L., Quigley, C., Thomas, P., Villarreal, J.C., Augustin, M.M., Barrett, M.D., Baucom, R.S., Beerling, D.J., Benstein, R.M., Biffin, E., Brockington, S. F., Burge, D.O., Burris, J.N., Burris, K.P., Burtet-Sarramegna, V., Caicedo, A.L., Cannon, S.B., Çebi, Z., Chang, Y., Chater, C., Cheeseman, J.M., Chen, T., Clarke, N. D., Clayton, H., Covshoff, S., Crandall-Stotler, B.J., Cross, H., dePamphilis, C.W., Der, J.P., Determann, R., Dickson, R.C., Di Stilio, V.S., Ellis, S., Fast, E., Feja, N., Field, K. J., Filatov, D.A., Finnegan, P.M., Floyd, S.K., Fogliani, B., García, N., Gâteblé, G., Godden, G.T., Goh, F. (Qi Y., Greiner, S., Harkess, A., Heaney, J.M., Helliwell, K.E., Heyduk, K., Hibberd, J.M., Hodel, R.G.J., Hollingsworth, P.M., Johnson, M.T.J., Jost, R., Joyce, B., Kapralov, M. V., Kazamia, E., Kellogg, E.A., Koch, M.A., Von Konrat, M., Könyves, K., Kutchan, T.M., Lam, V., Larsson, A., Leitch, A.R., Lentz, R., Li, F.W., Lowe, A.J., Ludwig, M., Manos, P.S., Mavrodiev, E., McCormick, M.K., McKain, M.,

McLellan, T., McNeal, J.R., Miller, R.E., Nelson, M.N., Peng, Y., Ralph, P., Real, D., Riggins, C.W., Ruhsam, M., Sage, R.F., Sakai, A.K., Scascitella, M., Schilling, E.E., Schlösser, E.M., Sederoff, H., Servick, S., Sessa, E.B., Shaw, A.J., Shaw, S.W., Sigel, E. M., Skema, C., Smith, A.G., Smithson, A., Stewart, C.N., Stinchcombe, J.R., Szövényi, P., Tate, J.A., Tiebel, H., Trapnell, D., Villegente, M., Wang, C.N., Weller, S.G., Wenzel, M., Weststrand, S., Westwood, J.H., Whigham, D.F., Wu, S., Wulff, A.S., Yang, Y., Zhu, D., Zhuang, C., Zuidof, J., Chase, M.W., Pires, J.C., Rothfels, C.J., Yu, J., Chen, C., Chen, L., Cheng, S., Li, J., Li, R., Li, X., Lu, H., Ou, Y., Sun, X., Tan, X., Tang, J., Tian, Z., Wang, F., Wang, J., Wei, X., Xu, X., Yan, Z., Yang, F., Zhong, X., Zhou, F., Zhu, Y., Zhang, Y., Ayyampalayam, S., Barkman, T.J., Nguyen, N. phuong, Matasci, N., Nelson, D.R., Sayyari, E., Wafula, E.K., Walls, R.L., Warnow, T., An, H., Arrigo, N., Baniaga, A.E., Galuska, S., Jorgensen, S.A., Kidder, T.I., Kong, H., Lu-Irving, P., Marx, H.E., Qi, X., Reardon, C.R., Sutherland, B.L., Tiley, G.P., Welles, S. R., Yu, R., Zhan, S., Gramzow, L., Theißen, G., Wong, G.K.S., 2019. One thousand plant transcriptomes and the phylogenomics of green plants. Nature 2019 574:7780 574, 679–685. Doi: 10.1038/s41586-019-1693-2.

Lengyel, S., Gove, A.D., Latimer, A.M., Majer, J.D., Dunn, R.R., 2010. Convergent evolution of seed dispersal by ants, and phylogeny and biogeography in flowering plants: a global survey. Perspect. Plant Ecol. Evol. Syst. 12, 43–55. https://doi.org/10.1016/J.PPEES.2009.08.001.

Li, H., 2013. Aligning sequence reads, clone sequences and assembly contigs with BWA-MEM. arXiv preprint arXiv:1303.3997. Doi: Doi: 10.48550/arXiv.1303.3997.

Li, H., Durbin, R., 2009. Fast and accurate short read alignment with Burrows-Wheeler transform. Bioinformatics 25, 1754–1760. https://doi.org/10.1093/BIOINFORMATICS/BTP324.

Li, H., Handsaker, B., Wysoker, A., Fennell, T., Ruan, J., Homer, N., Marth, G., Abecasis, G., Durbin, R., 2009. The sequence alignment/map format and SAMtools. Bioinformatics 25, 2078–2079. https://doi.org/10.1093/BIOINFORMATICS/BTP352.

Liberal, I.M., Burrus, M., Suchet, C., Thébaud, C., Vargas, P., 2014. The evolutionary history of *Antirrhinum* in the pyrenees inferred from phylogeographic analyses. BMC Evol. Biol. 14. https://doi.org/10.1186/1471-2148-14-146.

Llorens, L., 1982. Un nuevo endemismo de la isla de Menorca: *Apium bermejoi*. Folia Botanica Miscellanea 3, 27–33.

Loiseau, O., Mota Machado, T., Paris, M., Koubínová, D., Dexter, K.G., Versieux, L.M., Lexer, C., Salamin, N., 2021. Genome skimming reveals widespread hybridization in a neotropical flowering plant radiation. Front. Ecol. Evol. 9. https://doi.org/10.3389/FEVO.2021.668281/XML/NLM.

Lorite, J., March-Salas, M., et al., 2026. Expert-based classificaton of cliff flora: a case study in the iberian peninsula and balearic Islands. Sci. Data.

Losos, J.B., 2011. Convergence, adaptation, and constraint. Evolution 65, 1827–1840. https://doi.org/10.1111/J.1558-5646.2011.01289.X.

Ma, Y., Mao, X., Wang, J., Zhang, L., Jiang, Y., Geng, Y., Ma, T., Cai, L., Huang, S., Hollingsworth, P., Mao, K., Kang, M., Li, Y., Yang, W., Wu, H., Chen, Y., Davis, C.C., Shrestha, N., Ree, R.H., Xi, Z., Hu, Q., Milne, R.I., Liu, J., 2022. Pervasive hybridization during evolutionary radiation of *Rhododendron* subgenus *Hymenanthes* in mountains of southwest China. Natl. Sci. Rev. 9. https://doi.org/10.1093/NSR/NWAC276.

Maddison, W.P., 1997. Gene trees in species trees. Syst. Biol. 46, 523–536. https://doi.org/10.1093/SYSBIO/46.3.523.

Mallet, J., 2007. Hybrid speciation. Nature 2007 446:7133 446, 279–283. Doi: 10.1038/nature05706.

Mallet, J., Besansky, N., Hahn, M.W., 2016. How reticulated are species? Bioessays 38, 140–149. https://doi.org/10.1002/bies.201500149.

Matasci, N., Hung, L.H., Yan, Z., Carpenter, E.J., Wickett, N.J., Mirarab, S., Nguyen, N., Warnow, T., Ayyampalayam, S., Barker, M., Burleigh, J.G., Gitzendanner, M.A., Wafula, E., Der, J.P., dePamphilis, C.W., Roure, B., Philippe, H., Ruhfel, B.R., Miles, N.W., Graham, S.W., Mathews, S., Surek, B., Melkonian, M., Soltis, D.E., Soltis, P.S., Rothfels, C., Pokorny, L., Shaw, J.A., DeGironimo, L., Stevenson, D.W., Villarreal, J.C., Chen, T., Kutchan, T.M., Rolf, M., Baucom, R.S., Deyholos, M.K., Samudrala, R., Tian, Z., Wu, X., Sun, X., Zhang, Y., Wang, J., Leebens-Mack, J., Wong, G.K.S., 2014. Data access for the 1,000 Plants (1KP) project. GigaScience 3, 1–10. https://doi.org/10.1186/2047-217X-3-17/FIGURES/5.

Mayol, M., Rosselló, J.A., 2001. Seed isozyme variation in *Petrocoptis* A. Braun (Caryophyllaceae). Biochem. Syst. Ecol. 29, 379–392. https://doi.org/10.1016/S0305-1978(00)00067-3.

Mayol, M., Rosselló, J.A., 1999. A synopsis of *Silene* subgenus *Petrocoptis* (Caryophyllaceae). Taxon 48, 471–482. https://doi.org/10.2307/1224558.

McKenna, A., Hanna, M., Banks, E., Sivachenko, A., Cibulskis, K., Kernytsky, A., Garimella, K., Altshuler, D., Gabriel, S., Daly, M., DePristo, M.A., 2010. The genome analysis toolkit: a mapreduce framework for analyzing next-generation DNA sequencing data. Genome Res. 20, 1297–1303. https://doi.org/10.1101/GR.107524.110.

McLay, T.G.B., Birch, J.L., Gunn, B.F., Ning, W., Tate, J.A., Nauheimer, L., Joyce, E.M., Simpson, L., Schmidt-Lebuhn, A.N., Baker, W.J., Forest, F., Jackson, C.J., 2021. New targets acquired: Improving locus recovery from the Angiosperms353 probe set. Appl. Plant Sci. 9. https://doi.org/10.1002/APS3.11420.

Médail, F., Diadema, K., 2009. Glacial refugia influence plant diversity patterns in the Mediterranean Basin. J. Biogeogr. 36, 1333–1345. https://doi.org/10.1111/J.1365-2699.2008.02051.X.

Medail, F., Quezel, P., 1997. Hot-spots analysis for conservation of plant biodiversity in the mediterranean Basin. Ann. Mo. Bot. Gard. 84, 112. https://doi.org/10.2307/2399957.

Merxmüller, H., Grau, J., 1968. Ergänzende studien an *Petrocoptis* (Caryophyllaceae). Collect. Bot. 7, 787–797.

Minh, B.Q., Schmidt, H.A., Chernomor, O., Schrempf, D., Woodhams, M.D., Von Haeseler, A., Lanfear, R., Teeling, E., 2020. IQ-TREE 2: new models and efficient methods for phylogenetic inference in the genomic era. Mol. Biol. Evol. 37, 1530–1534. https://doi.org/10.1093/MOLBEV/MSAA015.

Moles, A.T., Westoby, M., 2004. Seedling survival and seed size: a synthesis of the literature. J. Ecol. 92, 372–383. https://doi.org/10.1111/J.0022-0477.2004.00884.X.

Molloy, E.K., Warnow, T., 2018. To include or not to include: the impact of gene filtering on species tree estimation methods. Syst. Biol. 67 (2), 285–303. https://doi.org/10.1093/sysbio/syx077. PMID: 29029338.

Montserrat, P., Fernández-Casas, J., 1990. *Petrocoptis* A. Braun, in: Castroviejo, S., Laínz, M., López-González, G., Montserrat, P., Muñoz-Garmendia, F., Paiva, J., Villar, L. (Eds.), Flora Iberica Vol.2. Real Jardín Botánico CSIC, Madrid, pp. 304–312.

Morales-Briones, D.F., Kadereit, G., Tefarikis, D.T., Moore, M.J., Smith, S.A., Brockington, S.F., Timoneda, A., Yim, W.C., Cushman, J.C., Yang, Y., 2021. Disentangling sources of gene tree discordance in phylogenomic data sets: testing ancient hybridizations in amaranthaceae s.l. Syst. Biol. 70, 219–235. https://doi.org/10.1093/SYSBIO/SYAA066.

Morales-Briones, D.F., Liston, A., Tank, D.C., 2018. Phylogenomic analyses reveal a deep history of hybridization and polyploidy in the Neotropical genus *Lachemilla* (Rosaceae). New Phytol. 218, 1668–1684. https://doi.org/10.1111/nph.15099.

Moreno, M.A., Holder, M.T., Sukumaran, J., 2024. DendroPy 5: a mature Python library for phylogenetic computing. J. Open Source Softw. 9, 6943. https://doi.org/10.21105/JOSS.06943.

Navarro, L., Guitián, J., 2002. The role of floral biology and breeding system on the reproductive success of the narrow endemic *Petrocoptis viscosa* Rothm. (Caryophyllaceae). Biol. Conserv. 103, 125–132. https://doi.org/10.1016/S0006-3207(01)00108-2.

Navarro, L., Guitian, J., Guitian, P., 1993. Reproductive biology of *Petrocoptis grandiflora* Rothm. (Caryophyllaceae), a species endemic to Northwest Iberian Peninsula. Flora 188, 253–261. https://doi.org/10.1016/S0367-2530(17)32274-0.

Nguyen, L.T., Schmidt, H.A., Von Haeseler, A., Minh, B.Q., 2015. IQ-TREE: a fast and effective stochastic algorithm for estimating maximum-likelihood phylogenies. Mol. Biol. Evol. 32, 268–274. https://doi.org/10.1093/MOLBEV/MSU300.

Ninyerola, M., Pons, X., Roure, J.M., 2005. Atlas climático digital de la Peninsula Ibérica. Metodología y aplicaciones en bioclimatología y geobotánica, Universtat Autonoma de Barcelona. Universitat Autónoma de Barcelona, Barcelona.

Nosil, P., 2012. Ecological Speciation. Oxford University Press.

Novikova, P.Y., Kolesnikova, U.K., Scott, A.D., 2022. Ancestral self-compatibility facilitates the establishment of allopolyploids in Brassicaceae. Plant Reproduction 2022 36:1 36, 125–138. Doi: 10.1007/S00497-022-00451-6.

Ortega-Olivencia, A., Rodríguez-Riaño, T., López, J., Valtueña, F.J., 2021. Elaiosome-bearing plants from the Iberian Peninsula and the Balearic Islands. Biodivers. Conserv. 30, 1137–1163. https://doi.org/10.1007/S10531-021-02137-3.

Pagel, M., 1999. Inferring the historical patterns of biological evolution. Nature 1999 401:6756 401, 877–884. Doi: 10.1038/44766.

Pamilo, P., Nei, M., 1988. Relationships between gene trees and species trees. Mol. Biol. Evol. 5, 568–583. https://doi.org/10.1093/OXFORDJOURNALS.MOLBEV.A040517.

Paradis, E., Schliep, K., 2019. ape 5.0: an environment for modern phylogenetics and evolutionary analyses in R. Bioinformatics 35, 526–528. https://doi.org/10.1093/BIOINFORMATICS/BTY633.

Peredo, E.L., Revilla, Á.M., Jiménez-Alfaro, B., Bueno, Á., Prieto, A.F.J., Abbott, R.J., 2009. Historical biogeography of a disjunctly distributed, Spanish alpine plant, *Senecio boissieri* (Asteraceae). Taxon 58, 883–892. https://doi.org/10.1002/TAX.583016.

Pirie, M.D., Humphreys, A.M., Barker, N.P., Linder, H.P., 2009. Reticulation, data combination, and inferring evolutionary history: an example from danthonioideae (Poaceae). Syst. Biol. 58, 612–628. https://doi.org/10.1093/SYSBIO/SYP068.

Pomeda-Gutiérrez, F., García, M.B., Leo, M., Fernández-Mazuecos, M., Alaoui, M.L., Terrab, A., Vargas, P., 2023. The pyrenees as a cradle of plant diversity: phylogeny, phylogeography and niche modeling of *Saxifraga longifolia*. J. Syst. Evol. 61, 253–272. https://doi.org/10.1111/JSE.12917/SUPPINFO.

Poplin, R., Ruano-Rubio, V., DePristo, M.A., Fennell, T.J., Carneiro, M.O., Auwera, G.A. Van der, Kling, D.E., Gauthier, L.D., Levy-Moonshine, A., Roazen, D., Shakir, K., Thibault, J., Chandran, S., Whelan, C., Lek, M., Gabriel, S., Daly, M.J., Neale, B., MacArthur, D.G., Banks, E., 2018. Scaling accurate genetic variant discovery to tens of thousands of samples. bioRxiv 201178. Doi: 10.1101/201178.

Purcell, S., Neale, B., Todd-Brown, K., Thomas, L., Ferreira, M.A.R., Bender, D., Maller, J., Sklar, P., De Bakker, P.I.W., Daly, M.J., Sham, P.C., 2007. PLINK: a tool set for whole-genome association and population-based linkage analyses. Am. J. Hum. Genet. 81, 559–575. https://doi.org/10.1086/519795.

R Core Team, 2025. R: A Language and Environment for Statistical Computing.

Revell, L.J., 2024. phytools 2.0: an updated R ecosystem for phylogenetic comparative methods (and other things). PeerJ 12, e16505. https://doi.org/10.7717/PEERJ.16505/FIG-22.

Revell, L.J., 2012. phytools: an R package for phylogenetic comparative biology (and other things). Methods Ecol. Evol. 3, 217–223. https://doi.org/10.1111/J.2041-210X.2011.00169.X.

Rhodes, J.A., Baños, H., Mitchell, J.D., Allman, E.S., 2021. MSCquartets 1.0: quartet methods for species trees and networks under the multispecies coalescent model in R. Bioinformatics 37, 1766–1768. https://doi.org/10.1093/BIOINFORMATICS/BTAA868.

Rieseberg, L.H., Soltis, D.E., 1991. Phylogenetic consequences of cytoplasmic gene flow in plants. Evol. Trends Plants 5, 65–84.

Rothmaler, W., 1941. Monographie der Gattung *Petrocoptis*. Bot. Jahrb. Syst. Pflanzengesch. Pflanzengeogr. 72, 117–130.

Sakamoto, Y., Ishiguro, M., Kitagawa, G., 1986. Akaike Information Criterion Statistics. D. Reidel, Dordrecht, The Netherlands.
Sang, T., Crawford, D.J., Stuessy, T.F., 1995. Documentation of reticulate evolution in peonies *(Paeonia)* using internal transcribed spacer sequences of nuclear ribosomal DNA: implications for biogeography and concerted evolution. Proc. Natl. Acad. Sci. 92, 6813–6817. https://doi.org/10.1073/PNAS.92.15.6813.
Scheunert, A., Heubl, G., 2017. Against all odds: reconstructing the evolutionary history of *Scrophularia* (Scrophulariaceae) despite high levels of incongruence and reticulate evolution. Org. Divers. Evol. 17, 323–349. https://doi.org/10.1007/S13127-016-0316-0.
Schiestl, F.P., Johnson, S.D., 2013. Pollinator-mediated evolution of floral signals. Trends Ecol. Evol. 28, 307–315. https://doi.org/10.1016/J.TREE.2013.01.019/ASSET/31F1709F-931D-4A6B-B6D1-15A4633E69C3/MAIN.ASSETS/GR1B1.SML.
Schluter, D., 2000. The Ecology of Adaptive Radiation. Oxford University Press.
Schuler, S.B.M., Hamza, H., Blanca, G., Romero-García, A.T., Suárez-Santiago, V.N., 2022. Phylogeographical Analyses of a Relict Fern of Palaeotropical Flora (*Vandenboschia speciosa*): Distribution and Diversity Model in Relation to the Geological and Climate Events of the Late Miocene and Early Pliocene. Plants 11. https://doi.org/10.3390/PLANTS11070839/S1.
Seehausen, O., 2013. Conditions when hybridization might predispose populations for adaptive radiation. J. Evol. Biol. 26, 279–281. https://doi.org/10.1111/JEB.12026.
Seehausen, O., 2004. Hybridization and adaptive radiation. Trends Ecol. Evol. 19, 198–207. https://doi.org/10.1016/J.TREE.2004.01.003/ASSET/CA695826-78D9-4E53-857E-FD859924B0CC/MAIN.ASSETS/GR5.SML.
Slater, G.S.C., Birney, E., 2005. Automated generation of heuristics for biological sequence comparison. BMC Bioinf. 6, 1–11. https://doi.org/10.1186/1471-2105-6-31/FIGURES/6.
Slimp, M., Williams, L.D., Hale, H., Johnson, M.G., 2021. On the potential of Angiosperms353 for population genomic studies. Appl. Plant Sci. 9. https://doi.org/10.1002/APS3.11419.
Sloan, D.B., Alverson, A.J., Wu, M., Palmer, J.D., Taylor, D.R., 2012. Recent acceleration of plastid sequence and structural evolution coincides with extreme mitochondrial divergence in the angiosperm genus *Silene*. Genome Biol. Evol. 4, 294–306. https://doi.org/10.1093/GBE/EVS006.
Slotte, T., Hazzouri, K.M., Ågren, J.A., Koenig, D., Maumus, F., Guo, Y.L., Steige, K., Platts, A.E., Escobar, J.S., Newman, L.K., Wang, W., Mandáková, T., Vello, E., Smith, L.M., Henz, S.R., Steffen, J., Takuno, S., Brandvain, Y., Coop, G., Andolfatto, P., Hu, T.T., Blanchette, M., Clark, R.M., Quesneville, H., Nordborg, M., Gaut, B.S., Lysak, M.A., Jenkins, J., Grimwood, J., Chapman, J., Prochnik, S., Shu, S., Rokhsar, D., Schmutz, J., Weigel, D., Wright, S.I., 2013. The *Capsella rubella* genome and the genomic consequences of rapid mating system evolution. Nature Genetics 2013 45:7 45, 831–835. Doi: 10.1038/ng.2669.
Smith, S.D., Kriebel, R., 2018. Convergent evolution of floral shape tied to pollinator shifts in Iochrominae (Solanaceae)*. Evolution (N Y). 72, 688–697. https://doi.org/10.1111/evo.13416.
Smith, S.D.W., 2010. Using phylogenetics to detect pollinator-mediated floral evolution. New Phytol. 188, 354–363. https://doi.org/10.1111/J.1469-8137.2010.03292.X.
Solís-Lemus, C., Ané, C., 2016. Inferring Phylogenetic Networks with Maximum Pseudolikelihood under Incomplete Lineage Sorting. PLoS Genet. 12, e1005896. https://doi.org/10.1371/JOURNAL.PGEN.1005896.
Soltis, D.E., Kuzoff, R.K., 1995. Discordance between nuclear and chloroplast phylogenies in the *Heuchera* group (Saxifragaceae). Evolution 49, 727–742. https://doi.org/10.1111/J.1558-5646.1995.TB02309.X.
Springer, M.S., Gatesy, J., 2016. The gene tree delusion. Mol. Phylogenet. Evol. 94, 1–33. https://doi.org/10.1016/J.YMPEV.2015.07.018.
Stamatakis, A., 2014. RAxML version 8: a tool for phylogenetic analysis and post-analysis of large phylogenies. Bioinformatics 30, 1312–1313. https://doi.org/10.1093/BIOINFORMATICS/BTU033.
Stebbins, G.L., 1970. Adaptive Radiation of Reproductive Characteristics in Angiosperms, I: Pollination Mechanisms. Annu. Rev. Ecol. Syst. 1, 307–326. https://doi.org/10.1146/annurev.es.01.110170.001515.
Swofford, D.L., 2003. PAUP*. Phylogenetic Analysis Using Parsimony (*and Other Methods).
Takebayashi, N., Morrell, P.L., 2001. Is self-fertilization an evolutionary dead end? Revisiting an old hypothesis with genetic theories and a macroevolutionary approach. Am. J. Bot. 88, 1143–1150. https://doi.org/10.2307/3558325.
Than, C., Ruths, D., Nakhleh, L., 2008. PhyloNet: a software package for analyzing and reconstructing reticulate evolutionary relationships. BMC Bioinf. 9, 1–16. https://doi.org/10.1186/1471-2105-9-322/TABLES/3.
Thiers, B., 2024. Index Herbariorum: A global directory of public herbaria and associated staff [WWW Document]. Index Herbariorum: A global directory of public herbaria and associated staff.New York Botanical Garden's Virtual Herbarium.
Trunschke, J., Sletvold, N., Ågren, J., 2017. Interaction intensity and pollinator-mediated selection. New Phytol. 214, 1381–1389. https://doi.org/10.1111/NPH.14479.
Upretee, P., Bandara, M.S., Tanino, K.K., Upretee, P., Bandara, M.S., Tanino, K.K., 2024. The Role of Seed Characteristics on Water Uptake Preceding Germination. Seeds 2024, Vol. 3, Pages 559-574 3, 559–574. Doi: 10.3390/SEEDS3040038.
Uyeda, J.C., Harmon, L.J., 2014. A Novel Bayesian Method for Inferring and Interpreting the Dynamics of Adaptive Landscapes from Phylogenetic Comparative Data. Syst. Biol. 63, 902–918. https://doi.org/10.1093/SYSBIO/SYU057.
Van der Auwera, G., O'Connor, B., Safari, 2020. Genomics in the Cloud: Using Docker, GATK, and WDL in Terra. O'Reilly Media 300.
Van der Niet, T., Johnson, S.D., 2012. Phylogenetic evidence for pollinator-driven diversification of angiosperms. Trends Ecol. Evol. 27, 353–361. https://doi.org/10.1016/J.TREE.2012.02.002.
Van Der Niet, T., Peakall, R., Johnson, S.D., 2014. Pollinator-driven ecological speciation in plants: new evidence and future perspectives. Ann. Bot. 113, 199–212. https://doi.org/10.1093/AOB/MCT290.
Vargas, O.M., Ortiz, E.M., Simpson, B.B., 2017. Conflicting phylogenomic signals reveal a pattern of reticulate evolution in a recent high-Andean diversification (Asteraceae: Astereae: *Diplostephium*). New Phytol. 214, 1736–1750. https://doi.org/10.1111/NPH.14530.
Walters, S.M., 1993. *Petrocoptis* A. Braun, in: Tutin, T.G., Heywood, V.H., Burges, N.A., Valentine, D.H., Walters, S.M., Webb, D.A. (Eds.), Flora Europaea Vol.1. Cambridge University Press, Cambridge, pp. 139–246.
Wen, D., Yu, Y., Nakhleh, L., 2016. Bayesian inference of reticulate phylogenies under the multispecies network coalescent. PLoS Genet. 12, e1006006. https://doi.org/10.1371/JOURNAL.PGEN.1006006.
Wen, D., Yu, Y., Zhu, J., Nakhleh, L., 2018. Inferring phylogenetic networks using phylonet. Syst. Biol. 67, 735–740. https://doi.org/10.1093/SYSBIO/SYY015.
Westoby, M., Leishman, M., Lord, J., 1996. Comparative ecology of seed size and dispersal. Philos. Trans. R. Soc., B 351, 1309–1318. https://doi.org/10.1098/RSTB.1996.0114.
Whitfield, J.B., Lockhart, P.J., 2007. Deciphering ancient rapid radiations. Trends Ecol. Evol. 22, 258–265. https://doi.org/10.1016/j.tree.2007.01.012.
Whitney, K.D., Ahern, J.R., Campbell, L.G., Albert, L.P., King, M.S., 2010. Patterns of hybridization in plants. Perspect. Plant Ecol. Evol. Syst. 12, 175–182. https://doi.org/10.1016/J.PPEES.2010.02.002.
Whittall, J.B., Hodges, S.A., 2007. Pollinator shifts drive increasingly long nectar spurs in columbine flowers. Nature 2007 447:7145 447, 706–709. Doi: 10.1038/nature05857.
Willis, K.J., Bennett, K.D., Walker, D., Hewitt, G.M., 2004. Genetic consequences of climatic oscillations in the Quaternary. Philos. Trans. R. Soc., B 359, 183–195. https://doi.org/10.1098/RSTB.2003.1388.
Wright, S.I., Kalisz, S., Slotte, T., 2013a. Evolutionary consequences of self-fertilization in plants. Proceedings of the Royal Society B: Biological Sciences 280. Doi: 10.1098/RSPB.2013.0133.
Wright, S.I., Kalisz, S., Slotte, T., 2013b. Evolutionary consequences of self-fertilization in plants. Proceedings of the Royal Society B: Biological Sciences 280. Doi: 10.1098/RSPB.2013.0133/74630.
Yang, L., Harris, A.J., Wen, F., Li, Z., Feng, C., Kong, H., Kang, M., 2023a. Phylogenomic analyses reveal an allopolyploid origin of core didymocarpinae (gesneriaceae) followed by rapid radiation. Syst. Biol. 72, 1064–1083. https://doi.org/10.1093/SYSBIO/SYAD029.
Yang, L., Shi, X., Wen, F., Kang, M., 2023b. Phylogenomics reveals widespread hybridization and polyploidization in *Henckelia* (Gesneriaceae). Ann. Bot. 131, 953–966. https://doi.org/10.1093/aob/mcad047.
Yu, Y., Nakhleh, L., 2015. A maximum pseudo-likelihood approach for phylogenetic networks. BMC Genomics 16, 1–10. https://doi.org/10.1186/1471-2164-16-S10-S10/COMMENTS.
Zhang, C., Rabiee, M., Sayyari, E., Mirarab, S., 2018. ASTRAL-III: polynomial time species tree reconstruction from partially resolved gene trees. BMC Bioinf. 19, 15–30. https://doi.org/10.1186/S12859-018-2129-Y/TABLES/2.
Zhang, C., Sayyari, E., Mirarab, S., 2017. ASTRAL-III: Increased scalability and impacts of contracting low support branches. Lecture Notes in Computer Science (including subseries Lecture Notes in Artificial Intelligence and Lecture Notes in Bioinformatics) 10562 LNBI, 53–75. Doi: 10.1007/978-3-319-67979-2_4/TABLES/3.
Zhou, X., Lutteropp, S., Czech, L., Stamatakis, A., Looz, M.V., Rokas, A., 2020. Quartet-Based Computations of Internode Certainty Provide Robust Measures of Phylogenetic Incongruence. Syst. Biol. 69, 308–324. https://doi.org/10.1093/SYSBIO/SYZ058.